6

Characterisation of the EL2 and E2 defects in n-GaAs

6.1 Introduction

One of the advantages of a digital DLTS system over an analogue system is that the digital DLTS system allows the observation of capacitance transients with time constants varying over several orders of magnitude. In order to test the DLTS system, it was decided to measure the emission of a defect over the widest possible temperature range. Both the EL2, in as-grown material, and the radiation-induced E2 defect in GaAs were measured over a wide temperature range. The results were compared to measurements obtained from an LIA-based DLTS system.

For the EL2 defect, the results obtained using digital DLTS corresponded well with those obtained previously using an analogue system. The experimental results were also close to previously published results. This was also true for the E2 at higher temperatures. However, below approximately 40 K, the emission rate of the E2 no longer decreased with decreasing temperature, but remained constant at roughly 1×10^{-3} s^{-1}. Further experiments indicated that the emission rate of this temperature-independent peak was not affected by the electric field effect.

These unexpected observations had not previously been reported in the literature, and a number of experiments were performed to ensure that the unusual results were not due to an artefact in the measuring system. After some experimentation, it was found that the observed emission was caused by blackbody radiation from the outer shroud of the cryostat that reached the sample through a hole in the radiation shield.

6.2 The EL2 and E2 defect levels in n-GaAs

The EL2 defect is probably the most extensively studied defect in GaAs. It is always present in as-grown GaAs in concentrations typically varying from 10^{15} to 10^{17} cm^{-3}. Despite the large amount of research done on the EL2, the atomistic origin of the defect level is not yet fully understood. However, it seems that it involves an arsenic anti-site defect (As_{Ga}) (Martin, 1986; Pons, 1985). The DLTS signature of the EL2 level in GaAs is reported in the literature as E_t = 0.825 eV and $\sigma_{na} = 1.2 \times 10^{-13}$ cm^2. (See Kaminska, 1999 for a detailed review.)

The E2 is one of a number of electron traps in GaAs induced by particle irradiation, and has been well characterised. It is a reasonably shallow energy level with E_t = 0.140 eV below the conduction band, with an apparent capture cross-section of $\sigma_{na} = 1 \times 10^{-13}$ cm^2. Structurally, the E2, as well as the shallower E1, are thought to be caused by two charge states of close arsenic vacancy–interstitial pairs (Pons, 1985). Both the E1 and E2 defect levels show field-enhanced emission that can be described by the phonon-assisted tunnelling model (Goodman, 1994).

A quick calculation shows that, under low electric field conditions, the E2 level's emission rate should vary from 10^3 s^{-1} to 10^{-4} s^{-1} in the temperature range 40 to 90 K. Since this temperature range is easily accessible by the cryostats in the Physics Department, the E2 seemed to be the ideal defect to use to test the capabilities of the DLTS system. The EL2 was chosen because it is a well-known defect, however, the maximum temperature restriction of the cryostat limited the emission rate range that could be measured.

6.3 Experimental

In this study, 1×10^{16} cm^{-3} Si-doped n-GaAs grown by OMVPE on an n^+ substrate was used. Ohmic contacts were fabricated on the back surface of the sample and 0.2 μm Au Schottky contacts were deposited by resistive evaporation, as described in Section 5.2. The sample was irradiated, through the Schottky contacts, by 5.4 MeV α-particles from an Am-241 source at a fluence of 1×10^{11} cm^{-2} for 8 hours. According to a TRIM simulation, these α-particles penetrate through the gold layer to a depth of 26 μm into the GaAs. Under a reverse bias of 1 V, a typical Au Schottky diode on 10^{16} cm^{-3}-doped GaAs has a depletion region width of about 0.5 μm. The electrically active defects produced by the α-particles during their travel though the GaAs should therefore be easily detectable by DLTS under various biasing conditions. A schematic representation of the sample is shown in Figure 6.1.

DLTS spectra of the samples were measured in an LIA DLTS system as well as in the digital DLTS system. In the case of the analogue system, LIA frequencies ranging from 1 Hz to 1 kHz were used, while, for the digital system, measurements were performed at temperatures ranging from 270 to 380 K for the EL2 and 20 to 90 K for the E2 defect. (Due to materials used in the construction of the interface, the EL2 could not be measured at temperatures over 380 K). In both cases, the scans were recorded at a reverse bias of 1 V and a filling pulse height of 1.2 V.

The field dependence of the emission from the E2 defect was studied using the digital system by applying a reverse bias of 4 V and increasing the filling pulse from 0.2 V to 3.4 V in 0.2 V steps.

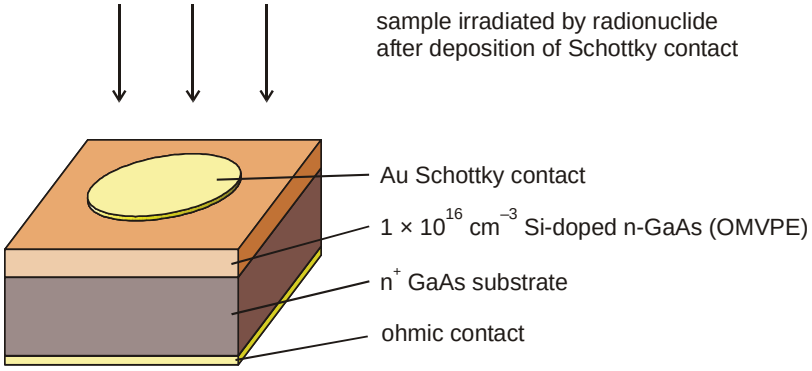

Figure 6.1 *Schematic representation of the sample used in this study.*

6.4 Results and discussion

Figure 6.2 compares the Arrhenius plots for the EL2 defect level as obtained by the two different systems. As seen in the graph, the digital system was capable of measuring the defect over a much wider range of emission rates. Over this wide range, no deviations from the linear relationship were observed. It can therefore be concluded that the digital system could measure long time constants accurately.

In the region where both systems could be used, the correspondence between the results was good. The DLTS signature obtained by the digital system (E_t = 0.833 eV and σ_{na} = 2.4 × 10^{-13} cm^2) corresponded reasonably well with the DLTS signature obtained by the analogue system (E_t = 0.785 eV and σ_{na} = 4.5 × 10^{-14} cm^2). Furthermore, the signature measured by the digital system was closer to the literature average mentioned in Section 6.2 (E_t = 0.825 eV and σ_{na} = 1.2 × 10^{-13} cm^2), than that obtained by the analogue system.

The difference in the results between the analogue and digital system seem to be due to a systematic deviation rather than due to random errors. The most probable cause for this systematic deviation is that the analogue system used an (uncalibrated) thermocouple to measure the temperature, while the temperature in the digital system was measured by a calibrated PT-100 sensor.

The results obtained by the digital DLTS system for the E2 level are shown in Figure 6.3. The emission rate from the E2 decreased as the temperature was decreased from 90 K to 40 K. However, when the temperature was decreased below 40 K, the emission rate from the E2 remained constant. In order to distinguish the peak showing a constant emission rate from the “normal” E2, the constant emission rate peak will be called E2'.

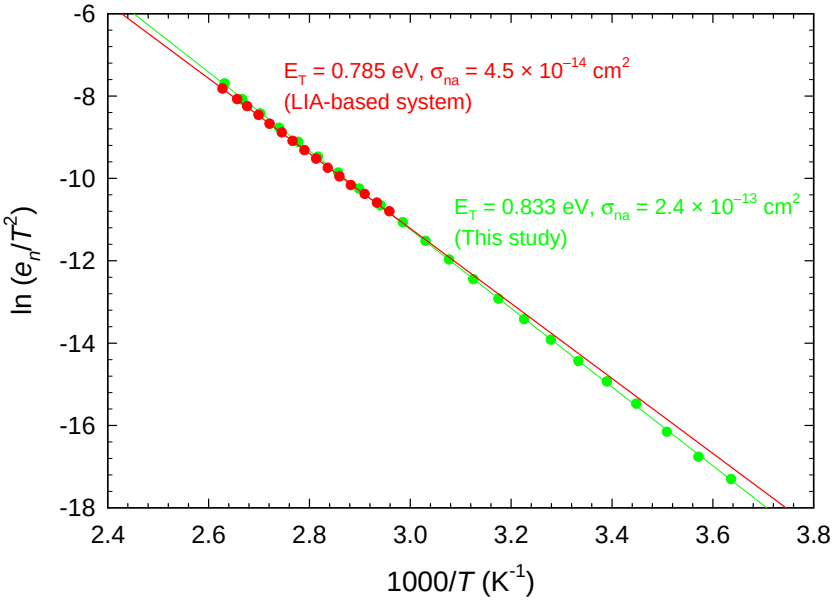

Figure 6.2 *Comparison of the Arrhenius plots obtained for the EL2 defect level as measured by the analogue as well as the digital DLTS system.*

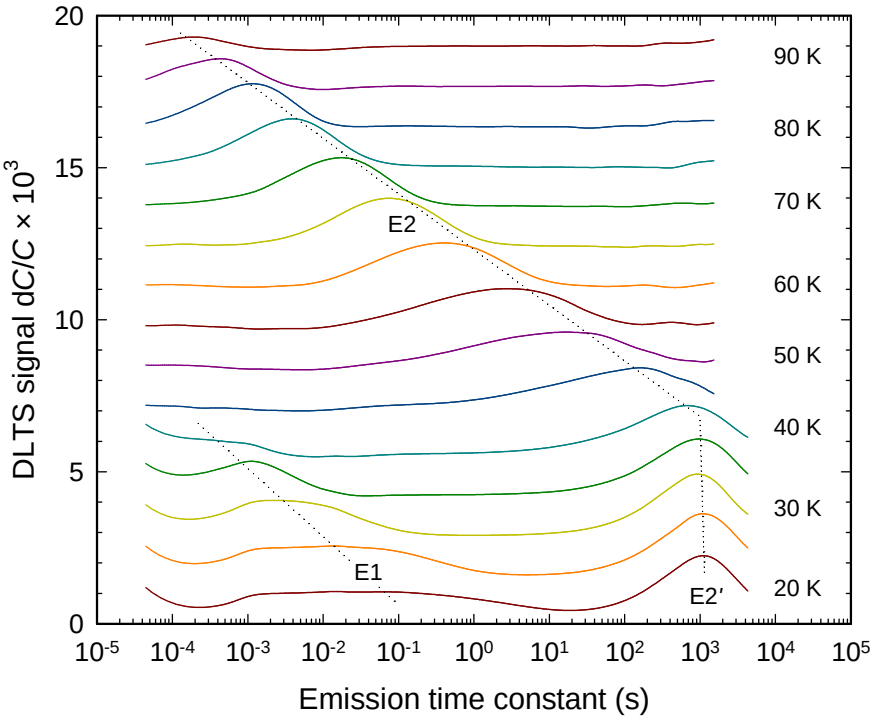

Figure 6.3 *Isothermal DLTS scans obtained from the sample at different temperatures. The bias conditions were: V_r = –1 and V_p = 1.2V. The broadening in the peaks is due to the electric field dependence of the emission rate, which becomes more pronounced at low temperatures.*

In the temperature range below 40 K, a peak due to the E1 was also visible. No unusual behaviour of the E1 was observed. The broadening in the peaks of both the E1 and the E2 was due to electric field enhanced emission. Note that the E2' peak did not show any signs of broadening.

It might be argued that, since the electric field remains approximately the same for all temperatures, the amount of broadening should also remain constant. However, in the lower temperature region, direct emission over the barrier becomes less important and the phonon-assisted tunnelling mechanism makes a significant contribution to carrier emission. Since phonon-assisted tunnelling is very sensitive to the electric field, it follows that, at lower temperatures, the varying electric field in the region probed by DLTS causes significant broadening of the DLTS peaks.

Figure 6.4 shows the dependence of the emission rate from the E2 on the temperature. At above 50 K, the log of the emission rate is approximately linearly dependent on 1/T, though at lower temperatures, the emission rate becomes practically independent of the temperature.

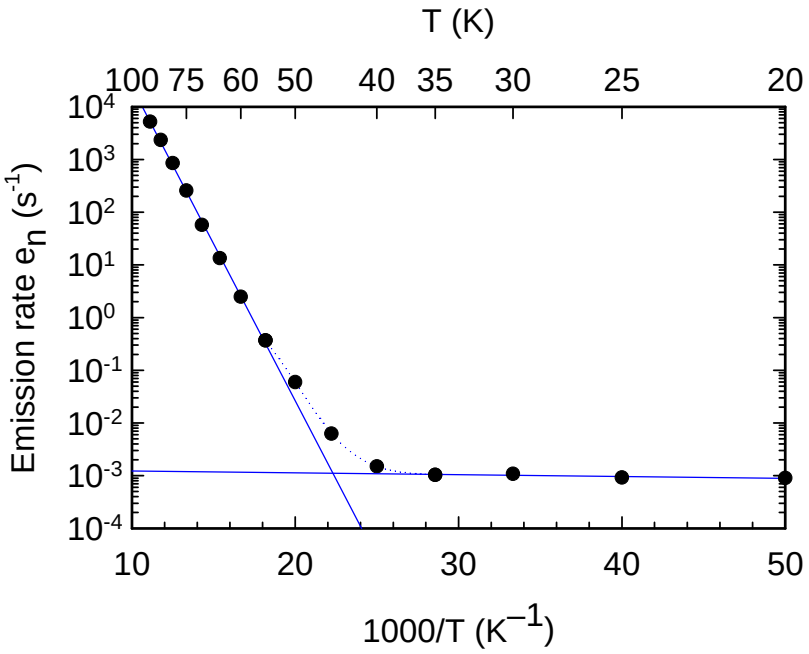

Figure 6.4 *Temperature dependence of the emission rate of the E2 level. (*V_r *= –1 V and* V_p *= 1.2 V, in* 1×10^{16} cm^{-3} *doped n-GaAs.)*

An Arrhenius plot of the data is shown in Figure 6.5. Here the data is compared to data obtained by an LIA based system in a previous study (Goodman, 1994). In the region above 50 K, the results agreed quite well, however, at 50 K a slight deviation is visible. Below 40 K the data was no longer described by Arrhenius' law, and therefore the temperature dependence of the emission rate from the defect could no longer be described by thermal emission according to Shockley-Read-Hall statistics.

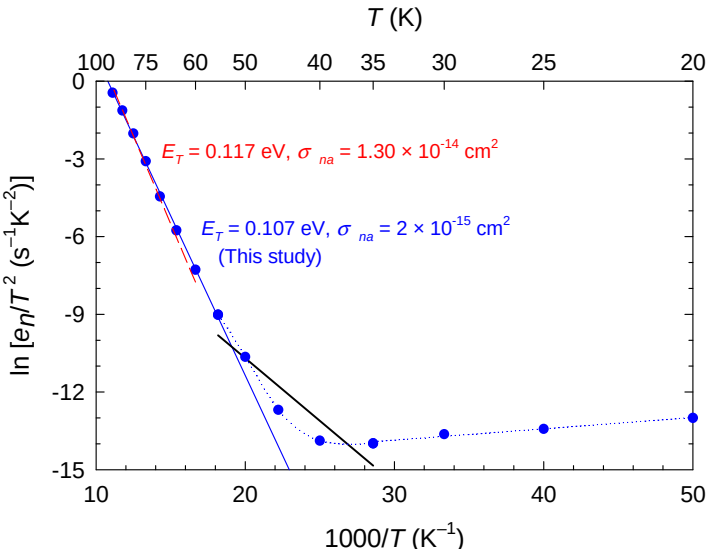

Figure 6.5 *Arrhenius plot of E2, obtained from the scans shown in Figure 6.3. The dashed line indicates results from Goodman (1994).*

Figure 6.6 shows digital DLTS spectra recorded at a reverse bias of 4 V and filling pulse amplitudes ranging from 0.2 V to 3.4 V incremented in 0.2 V steps. As the filling pulse amplitude was increased, defects closer to the surface were filled. These defects experienced a stronger field and therefore had a higher emission rate. Therefore, the DLTS peaks broadened to the left as the filling pulse was increased. Note that, in contrast to the E1, the E2' peak did not show any distortion due to the electric field until the filling pulse amplitude exceeded 2 V.

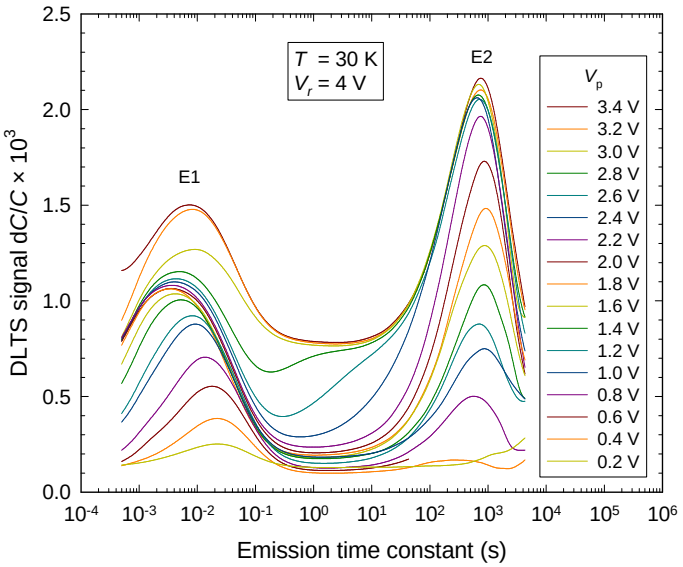

Figure 6.6 *Isothermal DLTS spectra of the E1 and E2 recorded at 30 K under a reverse bias of 4 V and filling pulse amplitudes ranging from 0.2 V to 3.4 V.*

In order to investigate the emission under a varying electric field, successive spectra in Figure 6.6 were subtracted. The result of this subtraction is shown in Figure 6.7, where the field dependence of the emission rate can be seen more clearly. Here it can be seen that the emission from the E2' remained independent of the electric field up to a field of 46 kV/cm after which the emission rate became strongly field dependent.

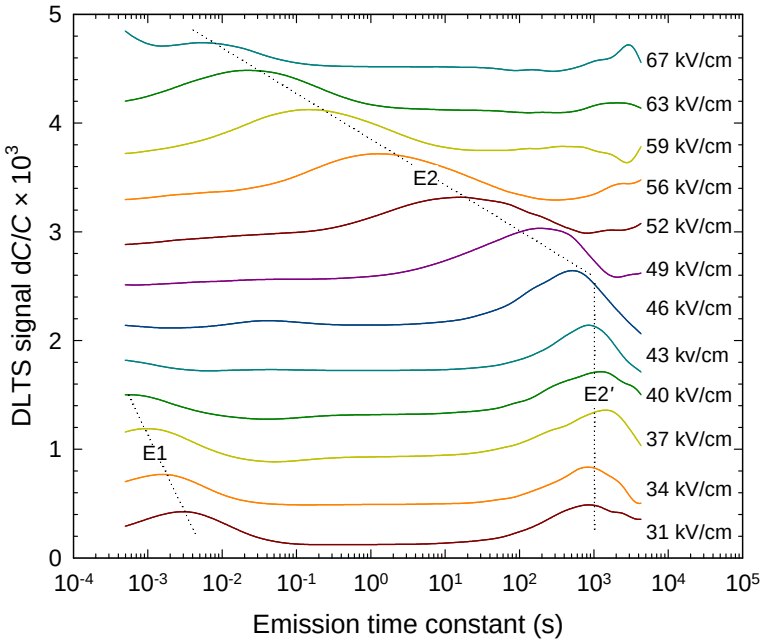

Figure 6.7 *Spectra obtained by subtracting successive scans in Figure 6.6. The average electric field experienced by the defects is also shown.*

The previous results strongly suggest that there was another mechanism according to which the E2 could emit carriers. This mechanism should be independent of temperature and electric field.

The radiation shield used in this study had a 10 mm hole in the top, for use in optical studies. When another radiation shield, without such a hole, was used, the E2' peak disappeared and was replaced with an E2 peak behaving as expected. The outer shroud of the cryostat was solid metal, so no ambient light could reach the sample. It is therefore thought that the observed emission of the E2 at low temperatures is due to blackbody radiation from the cryostat shroud.

A further investigation was done in which the top of the shroud was removed and replaced with an aluminium cap that was thermally insulated from the rest of the shroud. The bottom surface of the cap was sprayed with a carbon spray in order to approximate a blackbody radiator and a temperature sensor was attached to the cap. A 20-watt resistor was bolted on top of the cap to serve as a heater. In this way, using a second temperature controller, the temperature of the cap could be varied without affecting the rest of the set-up. It was found that the position of the peak due to the E2 shifted depending on the temperature of the cap, as shown in Figure 6.8. Note that only the position of the E2 peak shifts, therefore it is unlikely that the observed effect is due to a change in the temperature of the sample.

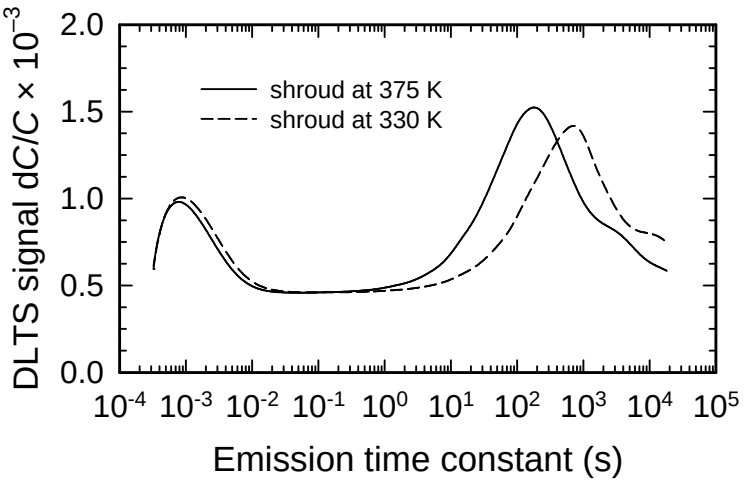

Figure 6.8 *Isothermal DLTS spectrum of the E1 and E2 levels recorded with the sample at 33 K and the cap of the radiation shield at different temperatures, showing the shift in the position of the peak due to the E2.*

6.5 Conclusions

The results obtained indicate that the digital DLTS system described can successfully measure defects with emission time constants ranging from 10^{-4} to more than 10^{3} s. The results obtained agreed well with results obtained previously using an LIA-based DLTS system, as well as with values published in the literature.

For very long time constants, deviations from the Arrhenius plot were observed, however, further investigations indicate that these deviations are due to blackbody radiation from the cryostat shroud.

6.6 Publications

Some of the results of this study were presented at the Conference on Photo-responsive Materials, Kariega Game Reserve, South Africa 25 – 29 February 2004 and published in Phys. Stat. Sol. (c) (Meyer, 2004):

1. Meyer WE and Auret FD 2004 Effect of thermal radiation on electron emission from the E2 defect in *n*-GaAs *Phys. Stat. Sol.* (c) **1** 2333

phys. stat. sol. (c) 1, No. 9, 2333–2336 (2004) / DOI 10.1002/pssc.200404850

Effect of thermal radiation on electron emission from the E2 defect in n-GaAs

W. E. Meyer* and **F. D. Auret**

Department of Physics, University of Pretoria, Pretoria, 0002, South Africa

Received 10 May 2004, revised 25 May 2004, accepted 2 June 2004
Published online 26 July 2004

PACS 71.55.Eq, 73.20.Hb

In this paper we describe the behaviour of the E2 defect in GaAs as measured by a digital DLTS system at temperatures much lower than those at which the defect is normally observed in analogue DLTS systems. We found that, at temperatures below approximately 40 K, the emission rate of the E2 defect became essentially temperature independent. We show that this behaviour is due to a competing mechanism, involving thermal radiation from the outer shroud of the cryostat, emptying the E2.

1 Introduction

The E2 defect level is one of the prominent electrically active radiation-induced defect levels in n-GaAs [1]. It can be observed by means of deep level transient spectroscopy (DLTS) [2] after irradiating n-GaAs with electrons, protons, α-particles and implantation with heavy nuclei [1, 3]. Under low-field conditions, the E2 has an energy level E_T and capture cross-section σ_{na} (collectively known as the defect's DLTS signature) of $E_C - 0.14$ eV and 1×10^{-13} cm^2 respectively in lowly doped material [1]. Emission from the E2 level is significantly enhanced by the electric field in the space charge region. This field-dependent emission is well described by the phonon assisted tunnelling model [4] with a Huang-Rhys factor, S, of 4.5 [5].

In this paper we present the results obtained when we investigated the emission from the E2 defect level at low temperatures (< 50 K) using a digital DLTS system, which is capable of measuring emission rates much lower than can be detected by traditional analogue systems.

2 Experimental

For this study we used <100> oriented GaAs epilayers grown by organo-metallic vapour phase epitaxy (OMVPE). The layers were grown on an n$^+$ substrate and had a free carrier concentration of 1×10^{16} cm^{-3} as determined by capacitance-voltage measurements. Ohmic contacts were fabricated on the back surface of the substrates and gold Schottky contacts, 0.7 mm in diameter and 0.2 μm thick, were evaporated resistively on the epilayer. The samples were irradiated through the evaporated contacts by 5.4 MeV α-particles from an Am-241 radionuclide.

Emission from the E2 was observed by means of a digital isothermal DLTS system in which the capacitance was measured using a Boonton 7200 capacitance meter. The capacitance signal was digitised by means of an HP3458A Multimeter. An HP33120A Arbitrary Waveform Generator provided the required reverse bias and filling pulses. The output of the HP33120A was found to be particularly stable with time, and did not suffer from baseline skew observed in some pulse generators. The use of an arbi-

* Corresponding author: e-mail: wmeyer@postino.up.ac.za

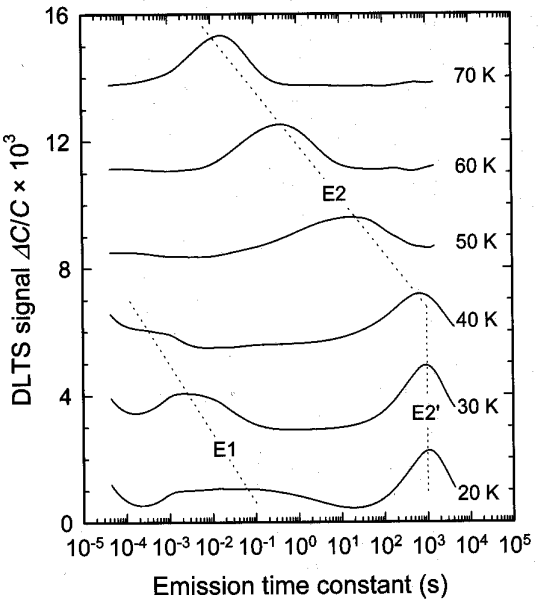

Fig. 1 Isothermal DLTS scans obtained at different temperatures. The bias conditions were: $V_r = -1$ and $V_p = 1.2$V.

trary waveform generator also allowed for the shaping of the filling pulse to minimise overshoot caused by the filters in the capacitance meter.

Initial measurements were performed without the inner shroud of the cryostat fitted. Hereafter, an inner shroud with its top removed was used. The top of the inner shroud was replaced with an aluminium disk that had a temperature sensor and a heater attached. The disk was isolated from the rest of the inner shroud by means of polystyrene foam. In order to provide a good blackbody radiator, the lower surface of the disk was painted with black colloidal graphite paint.

3 Results and discussion

Figure 1 shows the DLTS spectrum obtained at six different temperatures, without the inner shroud fitted. The curves recorded above 40 K clearly show that the emission rate from the E2 level decreased as the temperature was lowered. However, as the temperature was decreased to below 40 K, the emission rate of the E2 remained constant despite the temperature being lowered further (see the curves recorded at 20 and 30 K). In contrast to the behaviour of the E2 level, emission from the E1 level continued to decrease as the temperature was lowered.

The broadening of the E1 peak is due to field-enhanced emission, which generally becomes more pronounced at lower temperatures. At higher temperatures, the E2 peak is also broadened. However, at temperatures below 40 K, this broadening disappeared. The disappearance of the field-effect broadening of the peak indicates that the emission rate of the defect is not significantly influenced by the electric field.

Figure 2 shows an Arrhenius plot of the data obtained, and compares it to data measured previously in an LIA-based DLTS system. At higher temperatures (above 40 K), the results obtained compare well to those obtained in other studies, however, at low temperatures significant deviations were observed.

In order to ensure that these observations were not due to an artefact in the DLTS system, measurements were performed on the EL2 in the same sample over a similar emission rate range. No similar deviations were found.

From these results, we deduce that, besides the usual thermally stimulated emission mechanism, there is another mechanism that can empty the E2. This mechanism is slow ($e_n \sim 10^{-3}$ s^{-1}) and is essentially independent of temperature. At higher temperatures, the thermal emission process is much faster than the

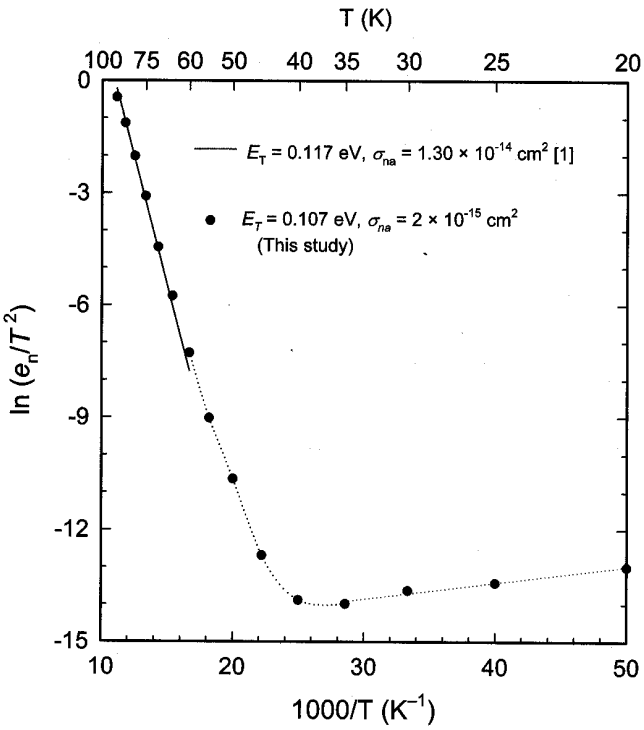

Fig. 2 Arrhenius plot of the data obtained in this study compared to data obtained in a previous study [1] in 10^{16} doped n-GaAs.

temperature independent mechanism, and the effects of the temperature independent mechanism are not observed. However, if the sample is cooled to below 40 K, the thermal emission process becomes slower than the temperature independent process. This causes the peak due to the thermal emission process to be replaced by one due to the temperature independent process.

We can also deduce that the temperature independent process is not significantly affected by the electric field in the depletion region, since the E2' peak does not show field-effect broadening.

After some experimentation, it was found that the temperature independent peak of the E2 defect disappeared when an inner shroud was fitted to the cryostat. Since there were no windows on the outer shroud of the cryostat, there was no light that could be shielded off by the inner shroud. The only radiation in the cryostat that might be blocked by the inner shroud is thermal radiation from the outer shroud. These results suggest that thermal radiation from the outer shroud is responsible for the temperature independent mechanism.

In order to investigate the possible effect of thermal radiation in more detail, a few measurements were performed with the top of the inner shroud heated to different temperatures. In this way it would be possible to investigate the effect of varying intensity thermal radiation on the sample. The results obtained in such a measurement are shown in Fig. 3, which shows some isothermal DLTS scans obtained at a measurement temperature of 33 K. In these scans, both the E1 and the E2 defects are observed. The position of the E1 does not change significantly, indicating that the sample temperature remained constant during the measurement. However, the position of the E2 level moves depending on the temperature of the top of the inner shroud. We therefore deduce that the E2' peak we observed, was due to thermal radiation from the outer shroud of the cryostat.

According to Wien's law, the peak emission of a black body radiator at 350 K is about 8 μm. This wavelength corresponds to a photon energy of 0.15 eV, which is approximately equal to the energy of the E2 below the conduction band (0.14 eV). Therefore, it seems plausible that the observed emission from the E2 may be due to these photons. It also explains why this phenomenon was not observed with the EL2 defect, which lies much deeper below the conduction band at 0.8 eV. From the above we expect that this phenomenon should be observed with other shallow defects where direct transitions are allowed.

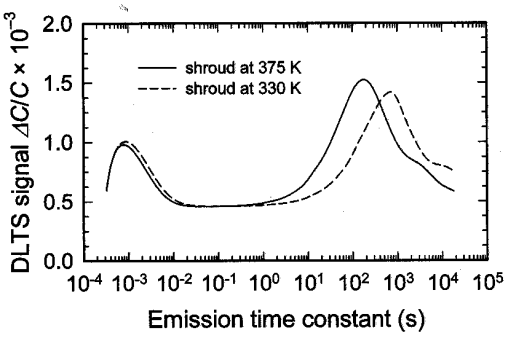

Fig. 3 Isothermal DLTS spectra recorded for the E1 and the E2 at 33 K with the top of the inner shroud heated to different temperatures.

4 Conclusion

We have shown that, under certain conditions, a temperature independent mechanism operates in addition to the usual thermal emission from the E2. At low temperatures, this temperature independent mechanism dominates over the thermal emission process, consequently only a single, temperature independent peak is observed. We have shown that this process is due to thermal radiation from the outer shroud of the cryostat, and expect the phenomenon to be observed in other shallow defects.

Acknowledgements The financial assistance of the NRF is gratefully acknowledged.

References

[1] S.A. Goodman, F.D. Auret, and W.E. Meyer, Nucl. Instr. and Meth. in Phys. Res. B **90**, 349 (1994).
[2] D.V. Lang, J. Appl. Phys. **45**, 3014 (1974)
[3] S.A. Goodman, F.D. Auret, and G. Myburg, Proc. Ninth Int. Conf. on Ion Beam Modification of Materials, Eds J.S. Williams, R.G. Elliman, and M.C. Ridgway (Elsevier, Amsterdam, 1995) p.866.
[4] D. Pons and S. Makram-Ebeid, J. Phys. (Paris) **40**, 1161 (1979).
[5] S.A. Goodman, F.D. Auret, and W.E. Meyer, Jpn. J. Appl. Phys. **33**, 1949 (1994).

7

Field dependence of the thermally activated emission rate

7.1 Introduction

In Section 2.2.3 a number of mechanisms according to which an applied electric field can enhance the emission of trapped carriers from a defect were discussed. It was mentioned that it is possible to determine a number of properties of a defect from the field dependency of its emission rate. For instance, the extent to which a defect displays the Poole-Frenkel effect is an indication of the approximate range of the defect's potential. This information can then be used to estimate the charge state of the defect and to determine whether the defect is an acceptor or a donor. At higher electric fields, many defects exhibit field-dependent emission enhancement that corresponds well with the phonon-assisted tunnelling model. In this case, curve-fitting routines can be used to determine the coupling constant between the lattice and the defect, the Huang-Rhys factor.

From a device viewpoint, it is also important to know the field-dependent emission properties of a defect. Since the application of an electric field may change the carrier emission rate of a defect by more than an order of magnitude, the electric field in a device may have significant impact on the way in which defects influence device performance.

The digital isothermal DLTS technique is ideally suited to the determination of the field dependence of the emission rate. The main advantage of this technique over the LIA-based technique is that all measurements are performed at the same temperature. It is therefore not necessary to use interpolation to estimate the emission rate of a defect at a given temperature. Furthermore, since the temperature remains constant, isothermal DLTS allows the temperature to be determined more accurately than with scanned temperature DLTS.

7.2 Publications

The digital DLTS system described in this thesis was used to determine the field dependence of a number of defects in different materials. The results of these studies are reported in the following publications, copies of which are included after this chapter. In all cases the isothermal DLTS measurements, the modelling and the curve fitting was performed by the present author.

1. Auret FD, Goodman SA and Meyer WE 1998 Field enhanced emission kinetics of an as-grown defect in RMBE grown n-GaN. *Proc. 24th Int. Conf. Phys. Semicond.* ed D Gershoni (Singapore: World Scientific)

2. Goodman SA, Auret FD, Meyer WE, Koschnick FK, Spaeth J-M, Beaumont B and Gibart P 1998 Deep level defects introduced in n-GaN by 5.4 MeV He-ions *Proc. 24th Int. Conf. Phys. Semicond.* ed D Gershoni (Singapore: World Scientific)

3. Goodman SA, Auret FD, Koschnick FK, Spaeth J-M, Beaumont B and Gibart P 1999 Field-enhanced emission rate and electronic properties of a defect introduced in n-GaN by 5.4 MeV He-ion irradiation *Appl. Phys. Lett.* **74** 809

4. Deenapanray PNK, Meyer WE and Auret FD 1999 Electric-field-enhanced emission and annealing behaviour of electron traps introduced in n-Si by low-energy He-ion bombardment *Semicond. Sci. Technol.* **14** 41

FIELD ENHANCED EMISSION KINETICS OF AN AS-GROWN DEFECT IN RMBE GROWN n-GaN

F.D. AURET, S.A. GOODMAN AND W.E. MEYER

Department of Physics, University of Pretoria, Pretoria, 0002, South Africa
E-mail: fauret@scientia.up.ac.za

We report on the enhanced emission kinetics of an as-grown defect in MBE grown n-GaN. This defect which is positioned 0.247 ± 0.005 eV below the conduction band and has an apparent capture cross-section of 3×10^{-13} cm^2. It exhibits an emission rate which depends on the electric field strength in the space-charge region. The emission rate increases from 6 s^{-1} at a field of 1×10^7 Vm^{-1} within the space-charge region to 10 s^{-1} when the electric field strength within this region is 5×10^7 V m^{-1}. This field dependence could not be explained by the Poole-Frenkel enhanced emission from a coulombic well, indicating that this defect is not a donor. This result does not support previously published results regarding the nature of this defect.

1 Introduction

An electric field can have a pronounced effect on emission from defects in semiconductors [1]. The negative aspect usually associated with electric field enhanced emission is that it results in inaccurate activation energy measurements and since the electric field increases with the doping density, this effect is especially pronounced in semiconductors with a carrier density above 10^{17} cm^{-3}. However, electric field assisted emission from deep level defects often assists in providing a better insight into several aspects of the defects being characterized. Firstly, if the Poole-Frenkel model for emission from a Coulomb potential can describe the enhanced emission data well, then it implies that the defect is a donor in n-type material, or an acceptor in p-type material. For example, the characteristic Poole-Frenkel field enhancement has been instrumental in identifying the inverted order of acceptor and donor levels of monatomic hydrogen in Si [2]. Secondly, it has been shown that the enhanced emission from some defects, including the well-known EL2 and some radiation-induced defects in GaAs, can be described by phonon-assisted tunneling. By fitting the experimental data to this model, the Huang-Rhys factor of the defect can be extracted from which one finds an indication of the lattice relaxation associated with carrier capture and emission.

In this paper, we investigate the electric field dependence of the emission rate of a defect in n-GaN grown by means of reactive molecular beam epitaxy (RMBE).

2 Experimental

For this study, 2 μm thick GaN epitaxial layers were grown on a 250 Å AlN buffer layer on sapphire by reactive molecular beam epitaxy (RMBE). The samples were cleaned in boiling aqua regia and degreased. Hereafter the oxide layer was removed using a 50% HCl solution for 10 seconds. Composite Ti/Al/Ni/Au (150 Å/2200 Å/ 400 Å/500 Å) ohmic contacts were deposited, followed by a 5 minute annealing at 500 °C in an inert atmosphere. Schottky contacts, 0.5 mm in diameter, were formed by resistively depositing 3000-Å gold through a mask. The carrier density of the material was determined by CV measurements as 2×10^{17} cm^{-3}.

Defect characterization was performed by means of a lock-in amplifier-based (LIA) deep level transient spectroscopy (DLTS) system. The DLTS signatures (energy level, E_T, and the apparent capture cross-section, σ_{na}) were determined at a quiescent reverse bias (V_r) of 1.0 V and a filling pulse (V_p) if 0.5 V. Isothermal DLTS, with a constant reverse bias and an incrementing filling pulse was used to determine the field dependence of the emission rate of the EM1. The results were analyzed according to the method of Zohta et al [3].

3 Results and discussion

The DLTS spectrum of the material shown in Figure 1 shows one dominant defect level, the EM1, which had an E_T and σ_{na} of 0.247 eV and 3×10^{-13} cm^2 respectively. The EM1 is presumably the same as the E_1 defect observed in RMBE grown GaN by Fang et al [4] with an E_T and σ_{na} equal to 0.21 eV and 1.26×10^{-14}. We ascribe the higher activation energy obtained by us to the lower electric field used in our measurements. Fang et al. speculated that, based on comparison between their data and that obtained for electron irradiated GaN, that E_1 is related to N-vacancies in GaN. Look et al. [5] have used Hall effect measurements to show that the N-vacancy in GaN is a donor-type defect.

In an attempt to determine the nature of the main defect observed in our study, the field dependence of the EM1 emission rate was determined. The results of these measurements are shown in Figure 2. In order to establish the potential associated with this defect the experimental data was modelled making use of various simple defect potential models. Since one-dimensional calculations grossly overestimate the field enhancement, we considered Poole-Frenkel enhancement from three-dimensional potentials only [6].

As shown in Figure 2, the data could not be explained by Poole-Frenkel enhancement from a coulombic well [7]. This dependence would imply that there is a coulombic attraction between the carrier and the defect, indicating that it is a donor in n-type material [8]. This is a strong indication that the defect is an acceptor.

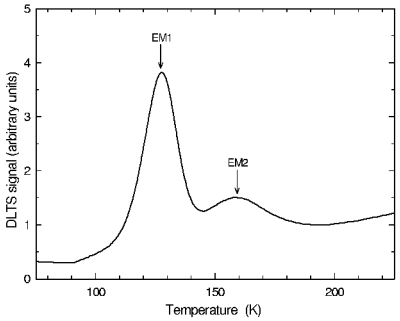

Figure 1. DLTS spectra of the as-grown sample. The spectrum was recorded at 46 Hz with V_r = 1.0 V and V_p = 1.2 V.

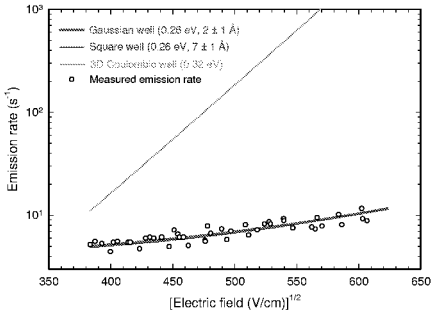

Figure 2. The experimental and modeled emission kinetics of the EM1 defect as a function of electric field strength in the space charge region.

A much better fit was obtained for a spherically symmetric square well [7] (depth 0.26 eV and radius 7 ± 2 Å) and a gaussian well [9] (depth 0.26 eV and characteristic width of 2 ± 0.5 Å). The difference between the field enhanced emission due to the gaussian well and that due to the square well was not large enough to allow a distinction to be made. However in both cases the dimensions of the well are of the order of a lattice parameter, therefore we conclude that the defect is a point defect. The slightly higher value of E_T determined from the modeling as compared to the experimental value is an indication that the defect energy determination was influenced by the high electric field in the highly doped material.

As mentioned previously, Fang et al. found a defect, the E_1, which we believe to be the same as the EM1 we observed. They suggest that the E_1 is related to the N-vacancy which is a donor-type defect. However, our results indicate that the EM1 defect is an acceptor. Therefore we have to assume that, either the EM1 we measured is not the same as the E_1, or the E_1 is not a donor and therefore not a N-vacancy.

4 Summary

We have determined the electronic properties of an as-grown defect in RMBE grown GaN which is positioned 0.247 eV below the conduction band with an apparent capture cross-section of 3×10^{-13} cm^2. Modeling of the emission kinetics in field strengths ranging from 1×10^5 to 4×10^5 V/cm has shown that the defect potential can not be described by a one- or a three-dimensional coulombic well. However, a square well with a depth of 0.26 eV and a radius of 7 ± 1 Å and a gaussian well of depth 0.26 eV and characteristic width 2.0 ± 1 Å both describe the enhanced emission very well. Hence we conclude from the physical dimensions of the modelled potential wells and the fact that EM1 does not exhibit the proportional

dependence on $F^{1/2}$ characteristic of a coulombic well that EM1 is a point defect which has acceptor like character.

Acknowledgments

We gratefully acknowledge the financial assistance of the South African Foundation for Research Development. We thank G. Myburg for assistance with the ohmic contact fabrication.

References

1. J. Frenkel, *Phys. Rev.* **54**, 657 (1938).
2. N.M. Johnson, C. Herring and C.G. van de Walle, *Phys. Rev. Lett.* **73**, 130 (1994).
3. Y. Zohta, and M.O. Watanabe, *J. Appl. Phys.* **53**, 1809 (1982).
4. Z-Q. Fang, D.C. Look, W. Kim, Z. Fan, A. Botchkarev and H Morkoç, *Appl. Phys. Lett.* **72** 2277 (1998).
5. D.C. Look, D.C. Reynolds, J.W. Hemsky, J.R. Sizelove, R.L. Jones, and R.J. Molnar, *Phys. Rev. Lett.* **79**, 2273 (1997).
6. N. Baber, and M.Z. Iqbal, *J. Appl. Phys.* **62**, 4471 (1987).
7. J. L. Hartke, *J. Appl. Phys.* **39**, 4871 (1968).
8. J. Bourgoin and M. Lannoo, Point Defects in Semiconductors II, Experimental Aspects, ed. M. Cardona (Springer Series vol. 35, Springer Verlag, 1983)
9. Q.S. Zhu, K. Hiramatsu, N. Sawaki, I. Akasaki, and X.N. Liu, *J. Appl. Phys.* **73**, 771 (1993).

DEEP LEVEL DEFECTS INTRODUCED IN n-GaN BY 5.4 MeV He-IONS

S.A. GOODMAN, F.D. AURET AND W.E. MEYER
Department of Physics, University of Pretoria, Pretoria, 0002, South Africa
E-mail: sgoodman@scientia.up.ac.za

F.K. KOSCHNICK AND J.-M. SPAETH
Fachbereich Physik, University of Paderborn, Paderborn, Germany

B. BEAUMONT AND P. GIBART
CRHEA-CNRS Valbonne, France

We have used deep level transient spectroscopy (DLTS) to characterise a deep level defect, the ER3, in unintentionally doped OMVPE grown GaN exposed to high energy (5.4 MeV) He-ions. The ER3 defect was introduced at a rate of 3270 ± 50 cm^{-1} and, under low electric field conditions, it has an energy level of 0.196 ± 0.004 eV below the conduction band and an apparent capture cross-section of 3.5 ± 1 × 10^{-15} cm^2. We found that the emission rate of the defect depends on the electric field strength in the space-charge region. This field dependence of the emission rate could be modelled according to the Poole Frenkel distortion of a square well with a radius of 20 ± 2 Å or a Gaussian well with a characteristic width of 6.0 ± 1 Å. Hence, we conclude that the ER3 is a point defect which appears to have acceptor like character.

1 Introduction

Gallium nitride, a direct wide bandgap semiconductor, has attracted considerable attention because of its applications in blue, green and ultraviolet light emitting diodes, detectors, and blue lasers. Because of its low thermal generation rates and high breakdown fields, an inherent property of wide bandgap semiconductors, it also has applications in the field of high temperature and power electronics [1]. The fabrication of electronic devices requires the definition of the device active area, which, for epitaxially based processes, is typically accomplished by mesa etching or implant isolation. It was found that He implantation-induced damage produced high resistivity GaN at a fluence that is compatible with photoresist masking techniques [2]. He-ion irradiation has the advantage over electron irradiation in its ability to isolate selected areas for device definition and is also suitable for carrier lifetime tailoring [3].

In this paper, we present the introduction rate and electrical properties of a deep level defect introduced by 5.4 MeV He-ions in n-GaN.

2 Experimental

For this study, 5μm thick GaN epitaxial layers were grown on a 250 Å buffer layer on sapphire by metal-organic vapour phase epitaxy (MOVPE) and exposed to 5.4 MeV He-ions from an ^{241}Am radio-nuclide source. The samples were cleaned in boiling aqua regia and degreased [4]. Hereafter the oxide layer was removed using a 50% HCl solution for 10 seconds [5]. Composite Ti/Al/Ni/Au (150 Å/2200 Å/ 400 Å/500 Å) ohmic contacts [6] were deposited, followed by a 5 minute annealing at 500 °C in an inert atmosphere. Schottky contacts, 0.5 mm in diameter, were formed by resistively depositing 3000 Å of gold through a mask.

Defect characterisation was performed by means of a lock-in-amplifier-based (LIA) deep level transient spectroscopy (DLTS) system. The DLTS signatures (energy level, E_T, and the apparent capture cross-section, σ_{na}) were determined at a quiescent reverse bias (V_r) of 1.0 V and a filling pulse (V_p) of 0.5 V. Isothermal DLTS, with a constant reverse bias and an incrementing filling pulse was used to determine the field dependence of the emission rate of ER3. The results were analyzed according to the method of Zohta et al [7].

3 Results and discussion

The DLTS spectrum of the as-grown material [Figure 1 curve (a)] contained two defect levels. The E02 had an E_T and σ_{na} of 0.27 eV and 8.85 × 10^{-15} cm^2 respectively while the E05 had an E_T and σ_{na} of 0.607 eV and 1 × 10^{-14} cm^2 respectively. The E02 and E05 defects are presumably the same as the E1 and E2 levels detected previously [8] in as-grown hydride vapour-phase epitaxially grown material.

After irradiation with He-ions, the DLTS spectrum [curve (b)] shows an additional defect, ER3, introduced at a rate of 3270 ± 200 cm^{-1} and positioned 0.196 ± 0.004 eV below the conduction band with an apparent capture cross-section of 3.5 × 10^{-15} cm^2. The electronic properties of the ER3 are similar to a defect found by Fang et al [9] in electron irradiated GaN, for which E_T and σ_{na} were 0.18 eV and 2.5 × 10^{-15} cm^2 respectively. The small discrepancy in the activation energy of the defects can be accounted for by field enhanced emission from the defect reported by Fang et al as their "signature" was determined under higher field conditions.

The field dependence of the emission from the defect is shown in Figure 2. In order to establish the potential associated with this defect the experimental data was modelled making use of various simple defect potential models. Since one-dimensional calculations grossly overestimate the field enhancement [10], we considered Poole-Frenkel enhancement from three dimensional potentials only.

As shown in Figure 2, the data could not be explained by Poole-Frenkel enhancement from a coulombic well [11]. This dependence would imply that there

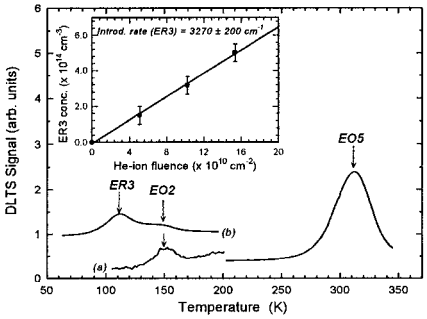

Figure 1. DLTS spectra of the unirradiated n-GaN [curve (a)] and the material exposed to 5.4 MeV He-ions [curve(b)]. The inset depicts the concentration of the He-ion induced defect ER3 a function of the incident He-ion fluence.

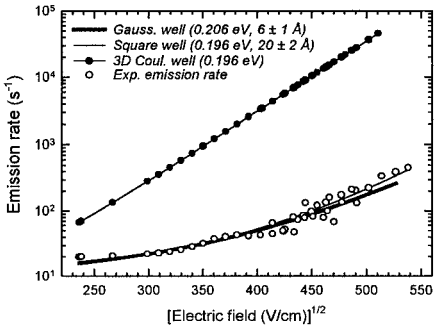

Figure 2. The experimental and modeled emission kinetics of defect ER3 as a function of electric field strength in the space charge region.

is a coulombic attraction between the carrier and the defect, indicating that it is a donor in n-type material [12]. We therefore assume that the defect is an acceptor. Further evidence for the acceptor nature of the ER3 are direct capture cross-section measurements which indicate a very low capture cross-section of 1×10^{17} cm^{-2}.

A much better fit was obtained for a spherically symmetric square well [11] (depth 0.196 eV and radius 20 ± 2 Å), while the best fit was obtained assuming a gaussian well [13] (depth 0.206 eV and characteristic width of 6.0 ± 1 Å). The difference between the field enhanced emission due to the gaussian well and that due to the square well was not large enough to allow a distinction to be made. However in both cases the dimensions of the well are of the order of a lattice parameter, therefore we conclude that the defect is a point defect.

We believe that the ER3 is the same defect as E previously observed by Fang et al. [9] who speculated that the defect may be related to the N-vacancy. However, Look et al. [14] have shown that the N-vacancy is a donor. This contradiction warrants further investigation.

4 Summary

We have determined the electronic properties of a defect introduced at a rate of 3270 ± 200 cm^{-1} by 5.4 MeV He-ions in n-GaN grown by OMVPE and is positioned 0.196 ± 0.004 eV below the conduction band. A defect with similar electronic properties and a considerably lower introduction rate has been observed after electron irradiation [9]. Modeling of the emission kinetics in field strengths ranging from 4.9×10^4 to 3×10^5 V/cm has shown that the defect potential is not a one- or a three-dimensional coulombic well. However, a square well with a depth of 0.196 eV and a radius of 20 ± 2 Å and a gaussian well of depth 0.206 eV and

characteristic width 6.0 ± 1 Å both describe the enhanced emission very well. Hence we conclude from the physical dimensions of the modelled potential wells and the fact that ER3 does not exhibit the proportional dependence on $F^{½}$, that ER3 is a point defect which has acceptor-like character.

Acknowledgments

We gratefully acknowledge the financial assistance of the South African Foundation for Research Development and the Forschungszentrum Jülich, International Bureau. We thank G. Myburg for assistance with the ohmic contact fabrication.

References

1. H. Morkoc, S. Strite, G.B. Gao, M.E. Lin, B. Sverdlov, and M. Burns, *J. Appl. Phys.* **76**, 1363 (1994).
2. S.C. Binari, H.B. Dietrich, G. Kelner, L.B. Rowland, K. Doverspike, and D.K. Wickenden, *J. Appl. Phys.* **78**, 3008 (1995).
3. D.C. Sawko, and J. Bartko, *IEEE Trans. Nucl. Sci.* **30**, 1756 (1983).
4. P. Hacke, T. Detchprohm, K. Hiramatsu, and N. Sawaki, *Appl. Phys. Lett.* **63**, 2676 (1993).
5. J.K. Sheu, Y.K. Su, G.C. Chi, W.C. Chen, C.Y. Chen, C.N. Huang, J.M. Hong, Y.C. Yu, C.W. Wang, and E.K. Lin, *J. Appl. Phys.* **83**, 3172 (1998).
6. S. Ruminov, Z. Liliental-Weber, J. Washburn, K.J. Duxstad, E.E. Haller, Z.-F. Fan, S.N. Mohammed, W. Kim, A.E. Botchkarev, and H. Morcoc, *Appl. Phys. Lett.* **69**, 1556 (1996).
7. Y. Zohta, and M.O. Watanabe, *J. Appl. Phys.* **53**, 1809 (1982).
8. P. Hacke, T. Detchprohm, K. Hiramatsu, N. Sawaki, K. Tadatomo, and K. Miyake, *J. Appl. Phys.* **76**, 304 (1994).
9. Z.-Q. Fang, J.W. Hemsky, D.C. Look, and M.P. Mack, *Appl. Phys. Lett.* **72**, 448 (1998).
10. N. Baber, and M.Z. Iqbal, *J. Appl. Phys.* **62**, 4471 (1987).
11. J. L. Hartke, *J. Appl. Phys.* **39**, 4871 (1968).
12. J. Bourgoin and M. Lannoo, Point Defects in Semiconductors II, Experimental Aspects, ed. M. Cardona (Springer Series vol. 35, Springer Verlag, 1983)
13. Q.S. Zhu, K. Hiramatsu, N. Sawaki, I. Akasaki, and X.N. Liu, *J. Appl. Phys.* **73**, 771 (1993).
14. D.C. Look, D.C. Reynolds, J.W. Hemsky, J.R. Sizelove, R.L. Jones, and R.J. Molnar, *Phys. Rev. Lett.* **79**, 2273 (1997).

APPLIED PHYSICS LETTERS VOLUME 74, NUMBER 6 8 FEBRUARY 1999

Field-enhanced emission rate and electronic properties of a defect introduced in *n*-GaN by 5.4 MeV He-ion irradiation

S. A. Goodman[a] and F. D. Auret
Physics Department, University of Pretoria, Pretoria, 0002, South Africa

F. K. Koschnick and J.-M. Spaeth
Fachbereich Physik, Universität GH Paderborn, Paderborn, Germany

B. Beaumont and P. Gibart
CRHEA-CNRS Valbonne, France

(Received 22 July 1998; accepted for publication 3 December 1998)

A deep level defect ER3, introduced in *n*-GaN by high energy (5.4 MeV) He ions, was characterized by deep level transient spectroscopy (DLTS). This defect, 0.196 ± 0.004 eV below the conduction band, with an apparent capture cross-section of $3.5\pm1\times10^{-15}$ cm^2, is introduced uniformly in the region profiled by DLTS at a rate of 3270 ± 200 cm^{-1}. The emission rate of this defect depends on the electric field strength in the space-charge region. This emission rate is modeled according to the Poole–Frenkel distortion of a square well with a radius of 20 ± 2 Å or alternatively, a Gaussian well with a characteristic width of 6.0 ± 1 Å. Hence, we conclude that ER3 is a point defect which has a field dependence not explained by the classical Poole–Frenkel enhancement. © *1999 American Institute of Physics.* [S0003-6951(99)02906-X]

Gallium nitride, a direct wide band gap semiconductor, has attracted considerable attention because of its applications in blue, green, and ultraviolet light emitting diodes, detectors, and blue lasers.[1] Because of its low thermal generation rates and high breakdown fields, an inherent property of wide band gap semiconductors, it also has applications in the field of high temperature and power electronics.[2] The fabrication of electronic devices requires the definition of the device active area. For epitaxially based processes, active area definition is typically accomplished by using mesa etching or implant isolation. Both H and He implantation damage has been used in GaN-based microelectronic processes.[3,4] It was found that He implantation-induced damage produced high resistivity GaN at a fluence that is compatible with photoresist masking techniques.[3] He-ion irradiation has the advantage over electron irradiation in its ability to isolate selected areas for device definition and also in carrier lifetime tailoring.[5] Deep level transient spectroscopy[6] (DLTS) is commonly used to study the electrical properties of deep levels within the space charge region of a Schottky barrier diode (SBD). It is generally assumed that the emission of carriers from deep levels is a purely thermal process. However, this may not always be the case and inaccurate defect characteristics may be calculated if one assumes only thermal emission. On the other hand, accurate measurements of the field enhancement of emission rates can lead to a model of the localized defect potential of the deep center thus providing vital insight into the nature of the defect states in the semiconductor.[7]

In this letter, we present the introduction rate, electrical properties, and the dependence of the emission rate on electric field strength of a deep level defect introduced by 5.4 MeV He ions in *n*-GaN.

For this study, GaN epitaxial layers 5 μm thick grown at 1080 °C on a 250 Å GaN buffer layer on sapphire by metal-organic vapor phase epitaxy (MOVPE) were exposed to 5.4 MeV He ions from a ^{241}Am radio-nuclide source. The nominally undoped GaN epitaxial layer had a free carrier concentration of approximately $2.2\pm0.2\times10^{16}$ cm^{-3}. After boiling the samples in aqua-regia for ten minutes the samples were degreased.[8] Prior to ohmic contact fabrication the oxide layer was removed from the sample surface using a HCl:H_2O (1:1) solution for 10 s.[9] The composite ohmic contact layer[10] was Ti/Al/Ni/Au (150 Å/2200 Å/400 Å/500 Å). The contact fabrication was followed by a five minute anneal at 500 °C in an inert gas atmosphere. Gold (Au) SBDs, 0.5 mm in diameter and 3000-Å-thick were resistively deposited, these diodes had a reverse leakage current of the order of 10^{-10} A at 1 V and ideality factors between 1.05 and 1.10. The samples were exposed to 5.4 MeV He ions by placing them on an ^{241}Am foil. The activity of the radionuclide being 192 μCi cm^{-2} and the dose rate was 7.1×10^6 cm^{-2} s^{-1}. A two-phase lock-in-amplifier-based (LIA) deep level transient spectroscopy (DLTS) system was used for the defect characterization. All DLTS ''signatures'' (activation energy, E_T and apparent capture cross-section, σ_{na}) were determined using a quiescent reverse bias (V_r) of 1.0 V and a filling pulse (V_p) of 0.5 V. DLTS depth profiling was performed by recording spectra at fixed quiescent reverse bias (V_r) but incrementing the forward bias (V_p) in small steps from one scan to the next. The approach of Zohta *et al.*[11] was then used to obtain the defect concentration as a function of depth below the interface. In order to simplify the determination of the emission kinetics of ER3 at different electrical field strengths in the space-charge region, isothermal DLTS was used.

Prior to He-ion irradiation, the MOVPE grown material contained two defects, $E02$ and $E05$ as illustrated in curve

[a]Electronic mail: sgoodman@nsnpert.up.ac.za

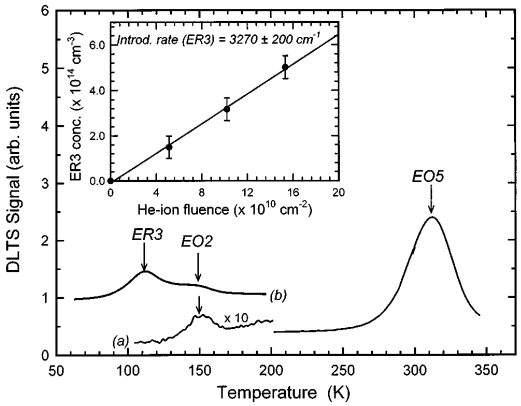

FIG. 1. DLTS spectra of the unirradiated n-GaN [curve (a)] and the material exposed to 5.4 MeV He ions [curve (b)]. The inset depicts the concentration of the He-ion induced defect ER3 as function of the incident He-ion fluence.

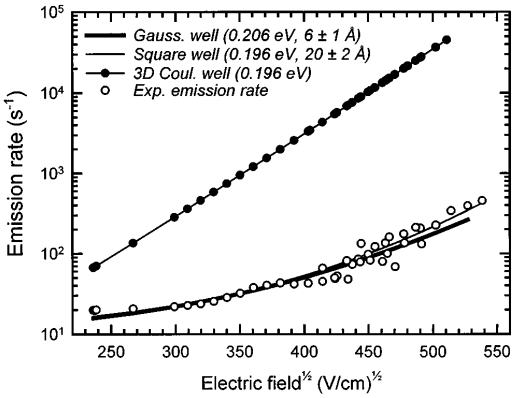

FIG. 2. The experimental and modeled emission kinetics of defect ER3 as a function of electric field strength in the space charge region.

(a) of Fig. 1. Defect $E02$, which is positioned 0.27 eV below the conduction band ($E_c-0.27$ eV) with an apparent capture cross-section of 8.5×10^{-15} cm^2, is believed to be the same as defect, $E1$[11] with a DLTS signature of 0.264 ± 0.01 eV and 1.6×10^{-15} cm^{-2} detected in as-grown hydride vapor-phase epitaxially grown material. A defect, E_2, has been detected in *unirradiated* MOVPE grown n-GaN, with an activation energy of 0.18 eV.[12] Defect $E05$, which has an activation energy of 0.607 eV with an apparent capture cross-section of 1×10^{-14} cm^2 is presumably the same as defect $E2$[13] detected in as-grown hydride vapor-phase epitaxially grown material with an activation energy of 0.580 ±0.017 eV with an apparent capture cross section of 2.9×10^{-15} cm^2.

After exposing n-GaN to 5.4 MeV He ions an additional defect, $ER3$ [curve (b), Fig. 1] was observed, this defect has a ''low field'' (7.6×10^4 V/cm) DLTS ''signature'' of $E_c-0.196\pm0.004$ and σ_{na} $3.5\pm1\times10^{-15}$ cm^2. There has been very few detailed investigations on the influence of particle irradiation on the electrical and optical properties of n-type GaN. Fang *et al.*,[14] irradiated n-GaN with 1 MeV electrons to a dose of 5×10^{14} and $\sigma_{na}1\times10^{15}$ cm^{-2}. A defect labeled E, for which the apparent parameters E_T and σ_{na} are 0.18 eV and 2.5×10^{-15} cm^2, respectively, was introduced at a rate of 0.2 cm^{-1}. It was speculated, taking into account the possibility of a temperature dependent capture cross-section, that this defect could possibly be the nitrogen vacancy (V_N, $E_c-0.07$ eV). The electronic properties of this defect and ER3 are similar. The small discrepancy in their activation energy could be accounted for by slight field enhanced emission of the defect reported by Fang *et al.*[14] as their defect ''signature'' was determined under higher electric field conditions.

In Fig. 2 the experimentally measured emission rate of ER3 as a function of the square root of the electric field in the space charge region is shown. In order to establish the potential associated with this defect the experimental data was modeled making use of various simple defect potential models. It must be noted, that the one-dimensional calculation grossly overestimated the field enhancement, as is well known.[15] Therefore, we firstly, consider the three-dimensional Poole–Frenkel description of electric field assisted thermal emission from a Coulombic well. According to this model,[16] the emission rate can be described by

$$e(F)=e(0)\left\{\left(\frac{kT}{\beta\sqrt{F}}\right)^2\left[1+\left(\frac{\beta\sqrt{F}}{kT}-1\right)\times e^{(\beta\sqrt{F}/kT)}\right]+\frac{1}{2}\right\}, \tag{1}$$

where $e(0)$ is the emission rate at zero electric field, k is Boltzmann's constant, T is the absolute temperature, and

$$\beta=\left(\frac{q^3}{\pi\epsilon}\right)^{1/2}. \tag{2}$$

It is evident from Fig. 2 that this particular potential does not suitably explain the experimentally measured emission enhancement. It must be noted that the characteristic dependence of the emission rate (e) on electric field (F) in the case of the one-dimensional Poole–Frenkel effect for a Coulombic well, namely that $\log e$ is proportional to $F^{1/2}$, is frequently used by experimentalists to distinguish between donor and acceptor defects. The linearity of this dependence is characteristic of a charge leaving a center of opposite sign. In n-type material this would imply a donor type defect, whereas, in p-type material this would imply an acceptor type defect.[7] It must be noted that the determination of the electronic type should be approached with caution as was expressed in the paper by Buchwald *et al.*,[17] who reported on the revised Poole–Frenkel effect for EL2 in GaAs.

Second, the Gaussian well was considered as a possible potential description for ER3. The enhanced emission rate in this case is[18]

$$e(F)=2\pi e(0)+\left\{\exp\left(\frac{V_0\exp(-r_0^2/\alpha^2)}{kT}\right)\frac{kT}{qFr_0}\times\left[\exp\left(\frac{qFr_0}{kT}\right)-1\right]+1\right\}, \tag{3}$$

where r_0 is the top of the distorted well where $\delta E/\delta r=0$. The resulting equation is nonlinear in r_0, F, α, and V_0, and has, therefore, been solved iteratively for each set of these

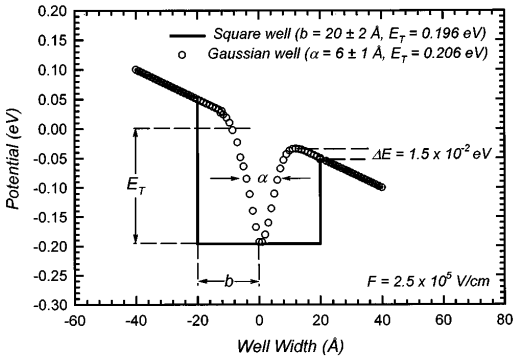

FIG. 3. The reduction in potential for a Gaussian and a square well, when the electric field strength in the space charge region is 2.5×10^5 V/cm.

values before calculating $e(F)$ using Eq. (3). A good fit is obtained when a characteristic width of 6.0 ± 1 Å and a potential of 0.206 eV is used.

Third, the spherically symmetric square well potential of radius b was investigated. The variation of emission rate $[e(f)]$ with electric field of a square well of radius b is[16]

$$e(F)=e(0)\{(kT/2qFb)[\exp(qFb/kT)-1]+1/2\}. \quad (4)$$

Using a potential equal to the experimentally determined activation energy, namely, 0.196 eV and a well with a radius of 20 ± 2 Å, a good fit is obtained between the experimentally measured emission rates and the modeled points.

It would appear that the square well and the Gaussian well with their particular physical dimensions discussed both provide an adequate description of defect ER3 detected after high energy He-ion irradiation. In an attempt to understand how both potentials describe the experimental results, a comparison of the distortion of these potentials at a reasonably high (2.5×10^5 V/cm) electric field strength was investigated. Figure 3 schematically represents the distortion of a square and a Gaussian well. It is clear from this figure that using either a Gaussian or a square well with the specified physical attributes can adequately describe the enhanced emission kinetics of ER3. The fact that the field enhanced emission from ER3 can not be adequately described by a Coulombic well indicates that ER3 is not a donor type defect but an acceptor type defect. The existence of another acceptor type defect not expected to exist in large numbers in as-grown material, namely, N_1 was experimentally shown by Look *et al.*[19]

In summary, we have determined the electronic properties of a defect introduced at a rate of $3270\pm200\,\mathrm{cm}^{-1}$ by 5.4 MeV He ions in n-GaN grown by organometallic vapor phase epitaxy (OMVPE). This defect which is positioned 0.196 ± 0.004 eV below the conduction band is introduced uniformly in the region probed by DLTS. A defect with similar electronic properties and a considerably lower introduction rate has been observed after electron irradiation.[12] Modeling of the emission kinetics in field strengths ranging from 4.9×10^4 to 3×10^5 V/cm has shown that the defect potential is not a one- or a three-dimensional Coulombic well. However, a square well with a depth of 0.196 eV and a radius of 20 ± 2 Å and a Gaussian well of depth 0.206 eV and characteristic width 6.0 ± 1 Å both describe the enhanced emission very well. Hence we conclude from the physical dimensions of the modeled potential wells and the fact that ER3 does not exhibit the proportional dependence on $F^{1/2}$ that is classically used to determine the electronic type of the defect.

The authors gratefully acknowledge the financial assistance of the South African Foundation for Research Development and the Forschungszentrum Jülich, International Bureau. They thank G. Myburg for assistance with the ohmic contact fabrication and W. E. Meyer for assistance with the isothermal DLTS measurements.

[1] S. Nakamura and G. Fasol, *The Blue Laser Diode* (Springer, New York, 1997).
[2] H. Morkoc, S. Strite, G. B. Gao, M. E. Lin, B. Sverdlov, and M. Burns, J. Appl. Phys. **76**, 1363 (1994).
[3] S. C. Binari, H. B. Dietrich, G. Kelner, L. B. Rowland, K. Doverspike, and D. K. Wickenden, J. Appl. Phys. **78**, 3008 (1995).
[4] S. J. Pearton, C. B. Vartuli, J. C. Zolper, C. Yuan, and R. A. Stall, Appl. Phys. Lett. **67**, 1435 (1995).
[5] D. C. Sawko and J. Bartko, IEEE Trans. Nucl. Sci. **30**, 1756 (1983).
[6] D. V. Lang, J. Appl. Phys. **45**, 3023 (1974).
[7] J. Bourgoin and M. Lannoo, *Point Defects in Semiconductors II, Experimental Aspects*, edited by M. Cardona, Springer Series, Vol. 35 (Springer, New York, 1983).
[8] P. Hacke, T. Detchprohm, K. Hiramatsu, and N. Sawaki, Appl. Phys. Lett. **63**, 2676 (1993).
[9] J. K. Sheu, Y. K. Su, G. C. Chi, W. C. Chen, C. Y. Chen, C. N. Huang, J. M. Hong, Y. C. Yu, C. W. Wang, and E. K. Lin, J. Appl. Phys. **83**, 3172 (1998).
[10] S. Ruminov, Z. Liliental-Weber, J. Washburn, K. J. Duxstad, E. E. Haller, Z.-F. Fan, S. N. Mohammed, W. Kim, A. E. Botchkarev, and H. Morcoç, Appl. Phys. Lett. **69**, 1556 (1996).
[11] Y. Zohta and M. O. Watanabe, J. Appl. Phys. **53**, 1809 (1982).
[12] W. Götz, N. M. Johnson, H. Amano, and I. Akasaki, Appl. Phys. Lett. **65**, 463 (1994).
[13] P. Hacke, T. Detchprohm, K. Hiramatsu, N. Sawaki, K. Tadatomo, and K. Miyake, J. Appl. Phys. **76**, 304 (1994).
[14] Z.-Q. Fang, J. W. Hemsky, D. C. Look, and M. P. Mack, Appl. Phys. Lett. **72**, 448 (1998).
[15] N. Baber and M. Z. Iqbal, J. Appl. Phys. **62**, 4471 (1987).
[16] J. L. Hartke, J. Appl. Phys. **39**, 4871 (1968).
[17] W. R. Buchwald and N. M. Johnson, J. Appl. Phys. **64**, 958 (1988).
[18] Q. S. Zhu, K. Hiramatsu, N. Sawaki, I. Akasaki, and X. N. Liu, J. Appl. Phys. **73**, 771 (1993).
[19] D. C. Look, D. C. Reynolds, J. W. Hemsky, J. R. Sizelove, R. L. Jones, and R. J. Molnar, Phys. Rev. Lett. **79**, 2273 (1997).

Semicond. Sci. Technol. **14** (1999) 41–47. Printed in the UK PII: S0268-1242(99)94350-X

Electric-field-enhanced emission and annealing behaviour of electron traps introduced in n-Si by low-energy He ion bombardment

P N K Deenapanray†‡, W E Meyer‡ and F D Auret‡

† Department of Electronic Materials Engineering, Australian National University, Canberra, ACT 0200, Australia
‡ Department of Physics, University of Pretoria, Pretoria 0002, South Africa

Received 15 May 1998, in final form 8 September 1998, accepted for publication 30 September 1998

Abstract. The isochronal annealing and electric-field-enhanced emission properties of three defects (EHe203, EHe584 and EHe211), observed in low-energy He-ion bombarded n-Si, were studied using deep level transient spectroscopy. EHe203 ($E_C - 0.20$ eV) and EHe584 ($E_C - 0.58$ eV) were thermally stable up to ~400 °C after which their removal was accompanied by the introduction of a secondary defect EHe211 ($E_C - 0.21$ eV). EHe211 was thermally stable at 650 °C. The emission rate of EHe203 was significant for electric fields above 4×10^4 V cm^{-1}, and was enhanced by over 3 orders of magnitude for a corresponding three-fold increase in electric field. The emission rate of EHe211 was only weakly field dependent over the electric field range studied, while that of EHe584 remained constant for electric fields between 3×10^4 and 9×10^4 V cm^{-1}. EHe584 has been proposed to be an acceptor-type defect. It was found that square wells of radii 57 Å and 40 Å described the potentials induced by EHe203 and EHe211, respectively, reasonably well. Alternatively, Gaussian potential wells with $\alpha = 20$ Å and $V_0 = 0.30$ eV (EHe203) and $\alpha = 12$ Å and $V_0 = 0.35$ eV (EHe211) could be used to fit our experimental data.

1. Introduction

Low-energy (0.2–2000 keV) noble gas ions (NGIs) are widely used during several microelectronics device fabrication steps, including ion beam etching, reactive ion etching and sputter deposition for metallization. The energetic ions create damage in the exposed semiconductor lattice through momentum transfer. This damage alters the electrical, optical and structural properties of the semiconductor and of devices fabricated thereon. For instance, the introduction of donor-type defects close to the crystal surface alters the barrier properties of Schottky barrier diodes fabricated on low-energy NGI-bombarded Si [1, 2]. Photoluminescence studies have shown that energy shifts in the no-phonon peak of the intrinsic I_1 defect (or W, 1.018 eV) occurred after bombarding Si with low-energy NGIs [3–5]. Those mass-dependent systematic line shifts were attributed to the incorporation of NGIs into the intrinsic defect, constituting a family of deep optical defects. Several conflicting models have been proposed for the structure of these NGI-related defects [6–8]. Using *ab initio* molecular dynamics modelling, Estreicher *et al* [9, 10] have recently proposed that the 1018 meV line was due to the neutral divacancy and that the shifted I_1 peaks were due to the incorporation of NGIs into the neutral divacancies. Despite these numerous studies, data concerning the electrical and annealing properties of deep level defects in low-energy NGI-bombarded Si are scarce.

Deep level transient spectroscopy (DLTS) [11] is commonly used to study the electrical properties of deep levels within the depletion region of a diode. It is commonly assumed that the emission of carriers from deep levels is a purely thermal process and that the internal electric field has no influence on the results. This is, however, not true and one is always cautioned against inaccurate findings from emission rate data if its dependence on electric field is not taken into account [11, 12]. The sensitivity of the emission rate to an applied electric field can be used to probe the range of a defect potential. Hence, an accurate measurement of the electric-field-enhanced emission rate from a deep level can provide valuable insight into the structure of processing-induced defects in semiconductor materials [13–15]. The successful assignment of a particular potential to a defect can be used as an input for further computer modelling of the defect structure [16].

Several studies to investigate the enhanced emission properties from defect levels in Si have made use of various defect potential models including, among others, the Poole–Frenkel coulombic well [17, 18], square well [18] and phonon assisted tunnelling [19, 20]. The one-dimensional

0268-1242/99/010041+07$19.50

Poole–Frenkel coulombic well, which relies on the linear dependence of the logarithm of the emission rate ($\ln(e)$) on the square root of electric field ($F^{1/2}$), has been the most widely used model since it enables one to distinguish whether a defect is an acceptor or donor [17]. This model has been used to describe the emission of electrons from the oxygen-related thermal donors [21] and chalcogen double donors [22] in silicon. A refinement on the one-dimensional model is the three-dimensional (3D) Poole–Frenkel coulombic potential well [18]. Walker and Sah [23] have used the spherical square well defect potential to study the electric-field-enhanced emission rate from deep levels observed in 1 MeV electron-irradiated silicon. The Gaussian well potential, which is less rigid than the square well model, has been used to study the vacancy-phosphorus-induced potential in InGaP [24].

In this paper we present results concerning the effect on an electric field on electron emission from three defects (EHe203, EHe584 and EHe211) observed in low-energy He-ion-bombarded n-Si. We show that the emission rates from EHe203 and EHe211 were enhanced by an externally applied electric field and that the effect was more pronounced for EHe203. The annealing properties of the defects are also reported. Furthermore, we demonstrate that the secondary defect EHe211 was introduced at the expense of EHe203 and EHe584 by annealing above ~400 °C.

2. Experimental procedure

Epitaxial Si, doped to 5×10^{15} P cm^{-3}, grown on an n$^+$-substrate by chemical vapour deposition, was used to investigate the annealing behaviour and electric-field-enhanced emission from EHe203, EHe584 and EHe211. The epitaxial side of the samples were bombarded with 1 keV He ions to a dose of 1×10^{12} cm^{-2} at room temperature. After chemical cleaning, Pd Schottky contacts 100 nm thick and 0.77 mm in diameter were deposited through a metal contact mask on the bombarded samples by resistive evaporation. Ohmic contacts (In–Ga eutectic mixture) were made on the n$^+$-side of the samples prior to electrical measurements.

Zero-bias (ZB) isochronal annealing was performed under Ar flow for 20 min periods from 100 to 650 °C in steps of 50 °C. DLTS spectra were recorded after each annealing cycle to monitor the defect annealing properties and the introduction of secondary defects. Difference DLTS (DDLTS) [25] was used to study the emission properties of the electron traps under externally applied electric fields. DDLTS yielded information about the defects located in a narrow spatial region, and was realized by subtracting DLTS spectra recorded at filling pulse amplitudes V_p and $V_p + \delta V_p$ (using a fixed quiescent bias V_r). The electric field dependence of the emission rates of EHe203 and EHe584 was measured on a sample annealed at 450 °C. By using $V_r = 5$ V and changing V_p from 0.5 to 5 V, the electric field could be varied between 5×10^4 and 1.5×10^5 V cm^{-1}. For EHe211, the electric field was varied between 2.5×10^4 and 4.5×10^4 V cm^{-1} by using $V_r = 2$ V and $0.5 \text{ V} \leqslant V_p \leqslant 2.3$ V. Because of the lower quiescent bias required to probe EHe211, we have used forward bias conditions to extend the electric field range. A sample annealed at 550 °C was used to measure the emission properties of EHe211.

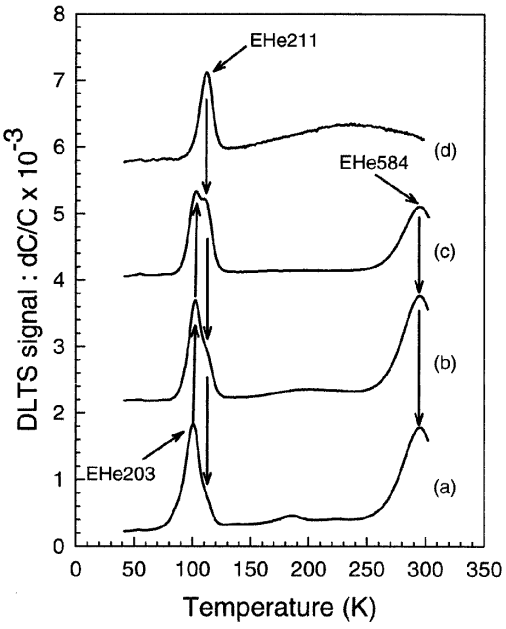

Figure 1. Curves a, b, c and d show the DLTS spectra of 1 keV He-ion-bombarded epitaxially grown n-Si (5×10^{15} cm^{-3}) after ZB isochronal annealing at 350, 450, 500 and 650 °C. The annealing was done under Ar flow for 20 min periods and in steps of 50 °C. EHe203 and EHe584 have a similar annealing behaviour. The high-temperature broad peak in curve d could be due to the degraded Schottky barrier diode or the presence of extended defects which introduced a continuous band of defects in the bandgap.

Free carrier compensation occurs in ion-beam-bombarded n-Si as a result of either the introduction of acceptor-type defects or dopant passivation in the form of dopant–defect pairs. This bombardment-induced lowering in dopant levels results in a corresponding decrease in the effective electric field experienced by deep traps. We have, therefore, computed the effective electric field in our samples using experimentally determined free carrier concentrations from variable-temperature capacitance–voltage (CV–T) measurement.

3. Results

3.1. Isochronal annealing behaviour

Figure 1 shows the DLTS spectra of 1 keV He-ion-bombarded n-Si after ZB isochronal annealing at 350, 450, 500 and 650 °C (curves a, b, c and d, respectively). It is evident from this figure that the annealing behaviours of EHe203 and EHe584 were similar. The high-temperature broad peak observed in figure 1, curve d, could be due to either the degraded metal–semiconductor interface at 650 °C or the presence of extended defects which introduced a continuous band of defects in the bandgap [26]. The variations in the peak DLTS intensities at a depth of 0.5 μm below the Pd–n-Si interface of EHe203 and EHe211 are illustrated in

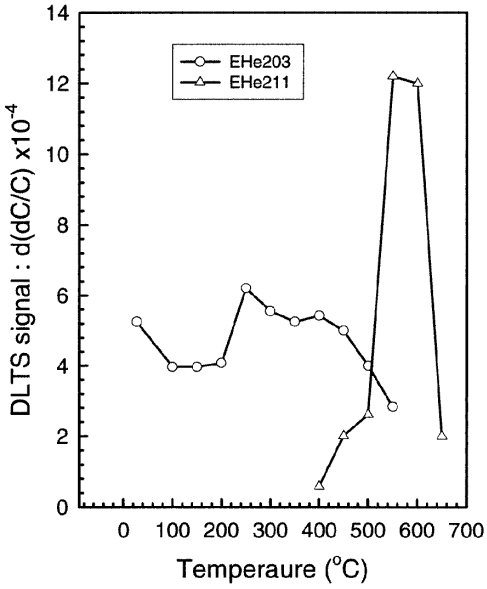

Figure 2. Variation in the peak DLTS intensities at a depth of 0.5 μm below the Pd–n-Si interface of EHe203 (open circles) and EHe211 (open triangles). The fading EHe203 signal peak above 550 °C was masked by the intense EHe211 peak and could not, therefore, be measured. It is clear that the removal of EHe203 was accompanied by the introduction of EHe211.

figure 2. The DLTS peak of EHe203 became weak above 550 °C and was masked by the dominant EHe211 signal peak. Figures 1 and 2 clearly demonstrated that the ZB isochronal annealing of EHe203 and EHe584 above 400 °C resulted in the simultaneous introduction of EHe211, which was thermally stable at 650 °C.

3.2. Dependence of emission rates on electric field

The emission rate of EHe584 showed virtually no electric field dependence. We observed a variation of 5% (within experimental error) in its value after changing the electric field from 3×10^4 to 9×10^4 V cm^{-1}. The variations in the emission rates of EHe203 and EHe211 as a function of applied electric field are shown in figures 3(a) and 3(b), respectively. The depth profiles of EHe203 and EHe211 (not shown) were determined using the method of Zohta and Watanabe [27]. Since the spatial distribution of EHe211 was shallower than that of EHe203, a smaller quiescent bias ($V_r = 2$ V compared with 5 V for EHe203) was used to study the electric field dependence of the emission property of EHe211. Figure 3(a) revealed that the emission rate of EHe203 was significantly enhanced by an electric field, while that of EHe211 showed a weak electric field dependence (figure 3(b)) over the electric field ranges covered in this study.

The low-field defect energy and apparent capture cross-section (E_t, σ_a) of the defects, commonly referred to as their DLTS 'signature', were extracted from the conventional DLTS Arrhenius plots [28] for the lowest electric fields. For

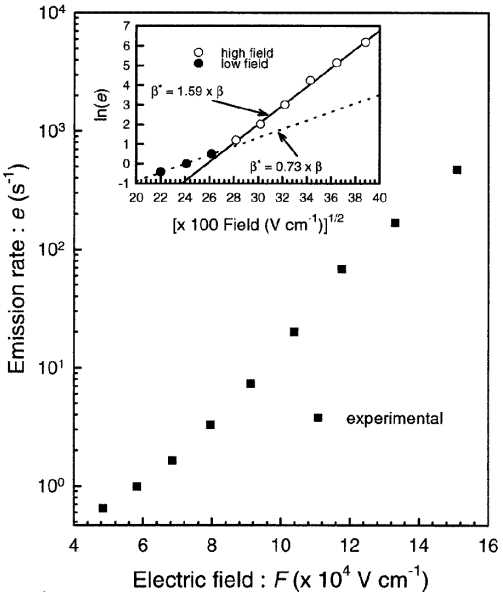

(a)

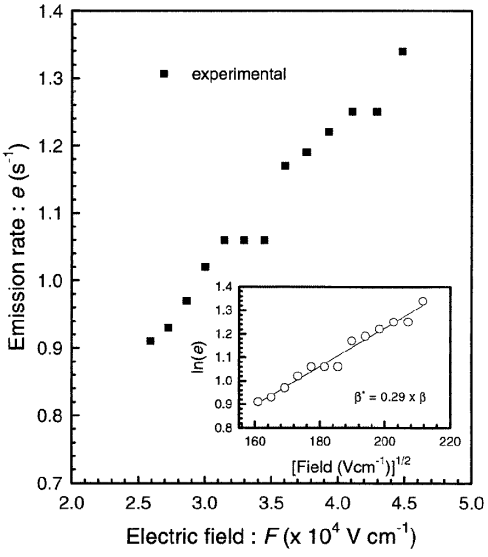

(b)

Figure 3. Variations in the emission rates of (a) EHe203 and (b) EHe211 as a function of externally applied electric field. The insets show linear plots of $\ln(e)$ versus $F^{1/2}$ for both defects, but the slopes did not yield the theoretical value of β for a singly charged defect. The emission rate data for EHe203 and EHe211 were measured at 85 and 100 K, respectively.

EHe203 and EHe211 the 'signatures' were 0.20 ± 0.03 eV, $(7.2 \pm 0.5) \times 10^{-16}$ cm^2 and 0.21 ± 0.03 eV, $(3.2 \times 0.5) \times 10^{-16}$ cm^2, respectively. The low-field 'signature' of EHe584 was 0.58 ± 0.03 eV and $(1.0 \pm 0.5) \times 10^{-15}$ cm^2. We have recently shown that the formation of EHe203

was independent of the presence of O, whereas EHe584 was introduced only in our O-containing samples. We have also proposed that the three electron traps investigated here were due to higher-order vacancy clusters [28–30]. The experimental data shown in figures 3(*a*) and 3(*b*) were simulated by employing the simple Poole–Frenkel coulombic, square and Gaussian defect potential models. The theoretical principles concerning the effects of an electric field on carrier emission from deep defect levels having potential wells of Coulomb, square and Gaussian forms have been described in [15] and will not be further discussed.

3.3. Coulombic potential well

According to the one-dimensional Poole–Frenkel formalism for a singly charged defect, a plot of $\ln[e(F)]$ versus $F^{1/2}$ should yield a straight line with slope β/kT [15, 17]. The plots of $\ln[e(F)]$ versus $F^{1/2}$ for EHe203 and EHe211 are depicted in the insets of figures 3(*a*) and 3(*b*), respectively. Although the experimental data could in both cases be closely fitted using linear regressions, the slopes of the linear fits did not yield the theoretical value of β for a singly charged defect. Figure 3(*a*) yielded experimental values β^* equal to 0.73β and 1.59β for the low- and high-field conditions, respectively, while figure 3(*b*) showed that a value of $\beta^* = 0.29\beta$ could be extracted. It followed that neither EHe203 nor EHe211 behaved according to the one-dimensional Poole–Frenkel formalism for a singly charged defect.

In order to simulate the expected field-dependent emission properties of EHe203 and EHe211 for one-dimensional Poole–Frenkel coulombic wells (figures 4 and 5, respectively), we have equated the zero-field emission rates ($e(0)$) of the traps to thermal emission rates (e(th)). The thermal emission rates, e(th), of EHe203 and EHe211 were calculated from their low-field 'signatures' using

$$e(\text{th}) = v_{th}\sigma_a N_C \exp(-E_t/kT) \qquad (1)$$

where v_{th} is the electron thermal velocity and N_C is the effective density of states in the conduction band. From curve a in figure 4 it is observed that the experimental data for EHe203 were a few orders of magnitude lower than the simulated data. In this case, the discrepancy between the experimental and simulated results could be reduced by using $\sigma_a \approx 10^{-18}$ cm^2 (curve b in figure 4), and changes in E_t did not have a significant effect (curve c in figure 4). Similarly, curves a, b and c of figure 5 further showed that the electric-field-enhanced emission rate from EHe211 could not be approximated by the one-dimensional Poole–Frenkel coulombic potential model. For any combination of E_t and σ_a, the increase in emission rate with increasing electric field was higher than the corresponding experimental increments.

A more comprehensive description of the electric-field-enhanced emission property from a singly charged particle (defect) can be described by the 3D coulombic well formalism [15, 18]. The field-assisted emission rates for 3D coulombic wells are illustrated by curves d and e in figures 4 and 5 for EHe203 and EHe211, respectively, Curve f in figure 4 corresponds to the simulation of the emission property for a double donor and is further discussed below. These curves showed that the electric-field-assisted emission

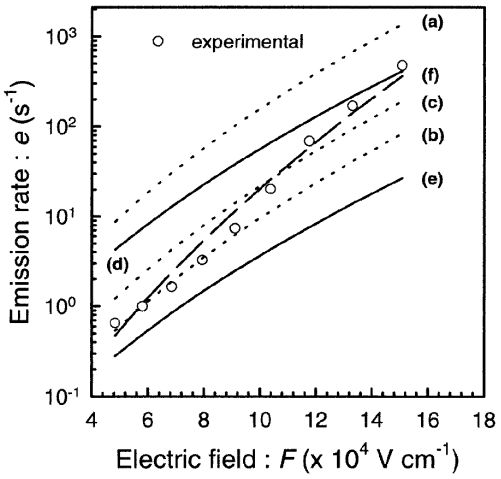

Figure 4. Experimental emission rate data (symbols) for EHe203 at a temperature of 85 K. Curves a–c (dotted lines) and d–f (full lines) are the modelled emission rates according to the Poole–Frenkel effect for one-dimensional and 3D coulombic potential wells, respectively. For the modelling we have used a low-field capture cross-section of 7.2×10^{-16} cm^2 (except for curve c) and the following values of E_t: curves a and c, $E_t = 0.20$ eV; curve b, $E_t = 0.22$ eV; curve d, $E_t = 0.19$ eV; curve e, $E_t = 0.21$ eV. Curve f is the emission rate data for a double donor for $E_t = 0.224$ eV. A value of $\sigma_a = 1 \times 10^{-16}$ cm^2 was used to model curve c. Curve c can be made to match curve b in the low-field region by using $\sigma_a = 5 \times 10^{-17}$ cm^2.

obtained for 3D coulombic wells were weaker than for the one-dimensional Poole–Frenkel effect, but nevertheless did not fit the experimental data. We have thus concluded that neither EHe203 nor EHe211 had pure coulombic wells associated with them.

3.4. Square and Gaussian wells

In contrast to the Coulombic well, a spherically symmetric square well potential (radius b) gives rise to a more rapid variation of emission rate with electric field [15, 18]. The depth of the square well was assigned by assuming that the measured thermal activation energy of the trapped electron (n-Si) was the ground-bound-state energy in the well [23]. A potential well which may be geometrically more realistic than the square well is the Gaussian well (depth of V_0 and a characteristic width α) [15, 24].

Curve b in figure 6 (dotted line) showed that a square well with $b = 57$ Å gave a reasonable fit to the experimental data for EHe203. The somewhat large value of b suggested that EHe203 was most probably not a point-like defect. The effect of varying the dimension of the square well is demonstrated by curves a and c. When fitting the Gaussian potential model to the experimental data of EHe203, values of 20 Å and 0.30 eV for α and V_0 ($E_t = 0.197$ eV), respectively (full line in figure 6) gave an identical fit to the square well model with $b = 57$ Å.

For EHe211 (figure 7), a value of $b = 40$ Å for a square well of depth 0.35 eV gave a reasonable fit to the experimental

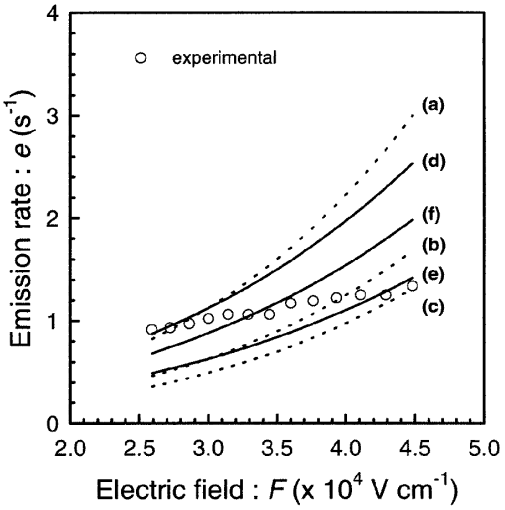

Figure 5. Experimental emission rate data (symbols) for EHe211 at a temperature of 100 K. Curves a–c (dotted lines) and d–f (full lines) are the modelled emission rates according to the Poole–Frenkel effect for one-dimensional and 3D coulombic potential wells, respectively. For the modelling we have used a low-field capture cross-section of 3.2×10^{-16} cm^2 (except for curves c and f) and the following values of E_t: curves a and c, $E_t = 0.23$ eV; curve b, $E_t = 0.235$ eV; curve d, $E_t = 0.215$ eV; curve e, $E_t = 0.22$ eV; curve (f), $E_t = 0.21$ eV. The effect of varying the capture cross-section is shown by curves c and f for which we have used $\sigma_a = 1.4 \times 10^{-16}$ cm^2.

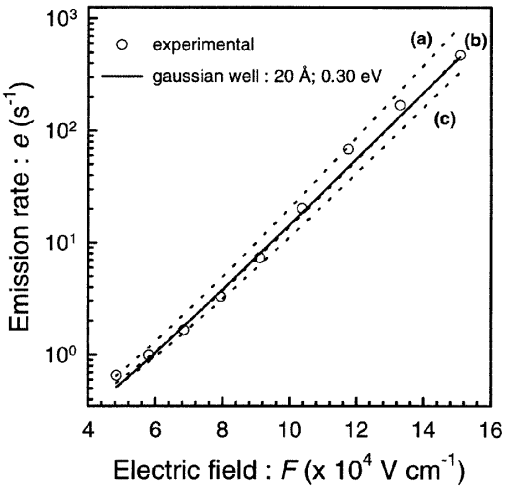

Figure 6. Modelled curves for a square well with three different dimensions for EHe203 (dotted lines). A value of $E_t = 0.185$ eV was used for curves a–c while the values of b were 60, 57 and 55 Å, respectively. The open circles represent the experimental data for EHe203 at 85 K. The curve drawn with a full line (overlaps with curve b) demonstrates that the experimental emission rate could also be simulated using the Gaussian potential model for $\alpha = 20$ Å, $V_0 = 0.30$ eV and $E_t = 0.197$ eV.

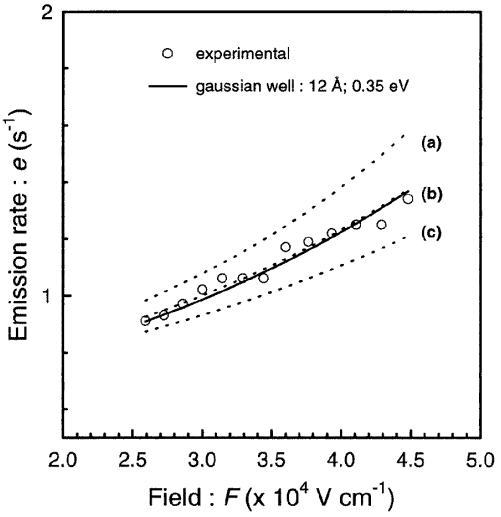

Figure 7. Modelled curves for a square well with three different dimensions for EHe211 (dotted lines). A value of $E_t = 0.197$ eV and $\sigma_a = 3.2 \times 10^{-16}$ cm^2 was used for curves a–c while the values of b were 45, 40 and 35 Å, respectively. The open circles represent the experimental emission rate for EHe211 at 100 K. The curve drawn as a full line (overlaps with curve b) demonstrates that the experimental emission rate could also be simulated using the Gaussian potential model for $\alpha = 12$ Å, $V_0 = 0.35$ eV and $E_t = 0.198$ eV.

data (curve b). The size of this potential well suggested that EHe211 was also not a point-like defect. The influence of changing the radius of the square well is illustrated by curves a and c. Similarly to EHe203, the experimental data for EHe211 could also be quite well fitted using the Gaussian well model. In this case, the dimensions of the Gaussian well were $\alpha = 12$ Å and $V_0 = 0.35$ eV ($E_t = 0.198$ eV), as shown by the full line in figure 7.

4. Discussion

The isochronal annealing behaviours of EHe203 and EHe584 were similar. Their concentrations as reflected by their peak DLTS intensities decreased after annealing above 400 °C. In this temperature range, the introduction of a secondary defect EHe211 was observed, and we have concluded that it was introduced, at least partially, at the expense of EHe203 and EHe584. This conclusion could be further supported by our isochronal annealing studies of 5.4 MeV α-particle- and Si-implanted epitaxially grown n-Si [28–30]. In those studies we had proposed that EHe203 was a vacancy cluster larger than the divacancy (V_x, $x > 2$) and EHe584 was a complex vacancy cluster involving O atoms (V_yO_z, $y > 2$). The annealing behaviour of EHe211 together with its high-temperature stability prompted us to believe that it was most probably a vacancy cluster larger than those responsible for EHe203 and EHe584. Annealing above 400 °C would cause the dissociation of EHe203 and EHe584 into smaller vacancy aggregates which would then diffuse and recombine to form the more thermally stable EHe211. It was recently shown that the reaction $V_{n-1} + V \rightarrow V_n$ was exothermic at least up

to $n = 7$ and that, except for the ring hexavacancy (V_6), V_n had several deep levels in the bandgap [10, 31].

The emission rate of EHe584 remained constant for electric fields in the range 3×10^4–9×10^4 V cm^{-1}. On the other hand, EHe203 showed significant electric-field-enhanced emission, whereby increasing the field threefold increased its emission rate by approximately 3 orders of magnitude. The emission rate of EHe211 was weakly field dependent between 2.5×10^4 and 4.5×10^4 V cm^{-1}.

The models that were explored to explain the emission enhancement of EHe203 and EHe211 were based on the Poole–Frenkel effect. Phonon-assisted tunnelling is characterized by the onset of a field-enhanced emission above a critical electric field (F_c). Since our experimental data did not show such a feature, it was clear that they could not be explained by pure phonon-assisted tunnelling.

The Poole–Frenkel effect has been widely used in the past to determine unambiguously whether a defect was of donor or acceptor type. It has, however, been demonstrated by Buchwald and Johnson [31] that short-range perturbations to the long-range coulombic tail, such as an energy barrier to carrier capture, could dramatically decrease the effect of externally applied electric fields on coulombic centres. Therefore, a null effect for the Poole–Frenkel effect did not unambiguously determine the defect type. In this study, because the emission property of EHe584 was electric field independent, and did not follow the Poole–Frenkel formalism, this defect was proposed to be acceptor type.

The potentials associated with EHe203 and EHe211 could not be explained using the coulombic potential model for a singly charged well (figure 3). Figures 4 and 5 revealed that large discrepancies (more pronounced for a one-dimensional well) existed between our experimental and simulated results when using the coulombic potential model. It is pointed out to the reader that the experimental value β^* can be used as an indication of the charge state of a defect. For example, a value of $\beta^* = \sqrt{2}\beta$ meant that the defect being investigated was a double donor (n-type semiconductor) [33]. Curve f in figure 4 revealed that EHe203 showed a field-enhanced emission property which was quite adequately described by the 3D Poole–Frenkel formalism for a double donor using $E_t = 0.224$ eV.

The potential wells induced by EHe203 and EHe211 were reasonably well explained using the square potential well formalism (figures 6 and 7, respectively). The radii of these wells ($b = 57$ Å for EHe203 and $b = 40$ Å for EHe211) revealed that the two defects had medium- to long-range potentials associated with them. Since the range of potentials for point-like defects usually extends only a few atomic spacings ($b < 10$ Å) [23], the experimental fit using the square potential well was in good agreement with our previous proposition that EHe203 and EHe211 were complex vacancy clusters [28–30]. Based on the above discussion, it can obviously be argued that the dimensions of the potential well associated with EHe211 ought to be larger than those of EHe203. We point out that the square well formalism does not account for defect charge states larger than unity [18]. Hence, we have speculated that the larger potential range of EHe203 was due to its higher charge state compared to EHe211.

The Gaussian potential well model also fitted the experimental data (figures 6 and 7) quite closely. However, the wells had small characteristic widths ($\alpha = 20$ Å and 12 Å) and depths $V_0 > E_t$ ($V_0 = 0.30$ eV and 0.35 eV) had to be used for modelling the field-assisted emission data. On the one hand, it might be tempting to conclude that these characteristic widths should correspond to those associated with point-like defect potential wells, which would be contradictory to the above explanations. On the other hand, it can be argued that, although the wells had small characteristics widths, they also had relatively larger depths V_0 (i.e. the electrons were not in the ground-bound-state of the Gaussian wells). One is, therefore, cautioned that since the Gaussian potential well has two moments (α, V_0) compared with one for the square potential well (b), a correlation between the dimensions of the Gaussian wells and the proposed physical structure of EHe203 and EHe211 was not straightforward. Furthermore, figures 6 and 7 revealed that, if the electrons were assumed to be in the ground-bound-state of the Gaussian potential wells ($E_t = V_0$), then the values of E_t required to model our experimental results adequately would have been larger than the measured low-field thermal activation energies of EHe203 and EHe584. However, similarly to what was observed using the square well model, our simulations showed that the width of the Gaussian potential well associated with EHe211 was smaller than that of EHe203.

5. Conclusions

In this paper we presented results concerning the isochronal annealing behaviour and electric-field-enhanced emission properties of three electron traps (EHe203, EHe584 and EHe211) introduced in 1 keV He-ion-bombarded epitaxially grown n-Si. EHe203 and EHe584 were found to behave similarly under ZB annealing. The removal of EHe203 and EHe584 by annealing above 400 °C was accompanied by the introduction of the secondary defect EHe211, which was thermally stable at 650 °C. The emission rate of EHe584 was independent of electric field and we have proposed that the defect was acceptor type. The emission rate of EHe203 was, on the other hand, significantly enhanced by an electric field. It showed an emission enhancement of approximately 3 orders of magnitude for a corresponding threefold increase in electric field. EHe211 showed only a weak field dependence. The potential wells associated with EHe203 and EHe211 could not be explained using the Poole–Frenkel coulombic potential model for a singly charged defect. However, the emission property of EHe203 followed that of a double-donor coulombic centre reasonably well.

The field-assisted emissions of EHe203 and EHe584 were described using the square well model with $b = 57$ Å and 40 Å, respectively. The size of the wells showed that the two defects had medium- to long-range potentials typical of non-point-like defects. This confirmed our previous propositions that EHe203 and EHe211 were complex vacancy clusters. The shorter potential range of EHe211 has been attributed to its smaller charge state. Gaussian potential wells with small characteristic widths but large depths ($V_0 > E_t$) could also be used to explain the emission properties of the two defects.

References

[1] Ashok S, Krautle H and Beneking H 1984 *Appl. Phys. Lett.* **45** 431
[2] Grussel E, Berg S and Andersson L P 1980 *J. Electrochem. Soc.* **127** 1573
[3] Weber J 1991 *Physica* B **170** 201
[4] Burger N, Thonke K, Sauer R and Pensl G 1984 *Phys. Rev. Lett.* **52** 1645
[5] Davis R J, Habermeier H-U and Weber J 1985 *Appl. Phys. Lett.* **47** 1295
[6] Sawyer W D, Weber J, Nabert G, Schmalzlin J and Habermeier H-U 1990 *J. Appl. Phys.* **68** 6179
[7] Kirkpatrick C G, Noonan J R and Streetman B G 1976 *Radiat. Eff.* **30** 97
[8] Minaev N S, Mudryi A V and Tkachev V D 1981 *Phys. Status Solidi* b **108** K89
[9] Estreicher S K, Weber J, Derecskei-Kovacs A and Marynick D S 1997 *Phys. Rev.* B **55** 5037
[10] Estreicher S K, Hastings J L and Fedders P A 1997 *Appl. Phys. Lett.* **70** 432
[11] Lang D V 1974 *J. Appl. Phys.* **45** 3014
[12] Tasch A F Jr and Sah C T 1970 *Phys. Rev.* B **1** 800
[13] Bourgoin J and Lannoo M 1983 *Point Defects in Semiconductor II, Experimental Aspects* (New York: Springer) pp 191–202
[14] Wang K L and Li G P 1983 *Solid State Commun.* **47** 233
[15] Auret F D, Goodman S A and Meyer W E 1995 *Semicond. Sci. Technol.* **10** 1376
[16] Estreicher S K and Fedders P A 1997 *Mater. Sci. Forum* **258–263** 171
[17] Frenkel J 1938 *Phys. Rev.* **54** 647
[18] Hartke J L 1968 *J. Appl. Phys.* **39** 4871
[19] Henry C H and Lang D V 1977 *Phys. Rev.* B **15** 989
[20] Pons D and Makram-Ebeid S 1979 *J. Phys. (Paris)* **40** 1161
[21] Kimerling L C and Benton J L 1981 *Appl. Phys. Lett.* **39** 410
[22] Pensl G, Roos G, Holm C and Wagner P 1986 *Mater. Sci. Forum* **10–12** 911–16
[23] Walker J W and Sah C T 1973 *Phys. Rev.* B **8** 5597
[24] Zhu Q S, Hiramatsu K, Sawaki N, Akasaki I and Liu X N 1993 *J. Appl. Phys.* **73** 771
[25] Lefevre H and Schultz M 1977 *Appl. Phys.* **12** 45
[26] Schröter W, Kronewitz J, Gnauert U, Riedel F and Seibt M 1995 *Phys. Rev.* B **52** 13 726
[27] Zohta Y and Watanabe M O 1982 *J. Appl. Phys.* **53** 1809
[28] Auret F D, Deenapanray P N K, Goodman S A, Meyer W E and Myburg G 1998 *J. Appl. Phys.* **83** 5576
[29] Deenapanray P N K, Auret F D and Ridgway M C 1998 *J. Appl. Phys.* **53** 1809
[30] Deenapanray P N K, Auret F D, Ridgway M C, Goodman S A and Myburg G 1998 *Mater. Res. Soc. Symp. Proc.* to be published
[31] Hastings J L, Estreicher S K and Fedders P A 1997 *Mater. Sci. Forum* **258–263** 509
[32] Buchwald W R and Johnson N M 1988 *J. Appl. Phys.* **64** 958
[33] Buchwald W R, Gerardi G J, Poindexter E H, Johnson N M, Grimmeiss H G and Keeble D J 1989 *Phys. Rev.* B **40** 2940